nature communications

Article

https://doi.org/10.1038/s41467-024-54031-5

# AS160 is a lipid-responsive regulator of cardiac $Ca^{2+}$ homeostasis by controlling lysophosphatidylinositol metabolism and signaling

Received: 13 March 2024

Accepted: 28 October 2024

Published online: 06 November 2024

Check for updates

Shu Su[1,2,11], Chao Quan[1,2,11], Qiaoli Chen[1,2,11], Ruizhen Wang[1,2], Qian Du[1,2], Sangsang Zhu[1,2], Min Li[1,2], Xinyu Yang[1,2], Ping Rong[1,2], Jiang Chen[3], Yingyu Bai[4], Wen Zheng[5,6], Weikuan Feng[1,2], Minjun Liu[1,2], Bingxian Xie[1,2], Kunfu Ouyang[7], Yun Stone Shi[1], Feng Lan[8], Xiuqin Zhang[5,6], Ruiping Xiao[5,6], Xiongwen Chen[4], Hong-Yu Wang[1,2,12] ✉ & Shuai Chen[1,2,9,10,12] ✉

The obese heart undergoes metabolic remodeling and exhibits impaired calcium ($Ca^{2+}$) homeostasis, which are two critical assaults leading to cardiac dysfunction. The molecular mechanisms underlying these alterations in obese heart are not well understood. Here, we show that the Rab-GTPase activating protein AS160 is a lipid-responsive regulator of $Ca^{2+}$ homeostasis through governing lysophosphatidylinositol metabolism and signaling. Palmitic acid/high fat diet inhibits AS160 activity through phosphorylation by NEK6, which consequently activates its downstream target Rab8a. Inactivation of AS160 in cardiomyocytes elevates cytosolic $Ca^{2+}$ that subsequently impairs cardiac contractility. Mechanistically, Rab8a downstream of AS160 interacts with DDHD1 to increase lysophosphatidylinositol metabolism and signaling that leads to $Ca^{2+}$ release from sarcoplasmic reticulum. Inactivation of NEK6 prevents inhibition of AS160 by palmitic acid/high fat diet, and alleviates cardiac dysfunction in high fat diet-fed mice. Together, our findings reveal a regulatory mechanism governing metabolic remodeling and $Ca^{2+}$ homeostasis in obese heart, and have therapeutic implications to combat obesity cardiomyopathy.

Obesity cardiomyopathy has been increasingly recognized as an obesity complication that develops myocardial dysfunction, independent of hypertension and coronary heart disease[1,2]. Complex mechanisms are involved in the pathogenesis of obesity cardiomyopathy involving in structural, biochemical, molecular and functional alterations, which have not been well understood so far.

The heart undergoes the contraction/relaxation cycle that is an energy-demanding process and controlled by shuttling of calcium ($Ca^{2+}$) between the cytosol and sarcoplasmic reticulum (SR). In face of fluctuation of nutrients under various conditions, the heart is metabolically flexible in the utilization of different substrates such as glucose, fatty acids and ketone body for energy production. For example, the heart in obesity undergoes metabolic remodeling with increased fatty acid oxidation and decreased glucose utilization[3,4]. Persistent cell surface relocation of an insulin-sensitive fatty acid translocase CD36 underlies the increase of fatty acid oxidation in the heart of diet-induced obese rats[5]. Excess fatty acids and their metabolic products such as ceramides and diacylglycerols consequently cause lipotoxicity to cardiomyocytes and lead to cardiac insulin resistance[3]. Insulin resistance in turn decreases glucose uptake into cardiomyocytes through inhibiting insulin-stimulated trafficking of the key glucose transporter GLUT4 in cardiomyocytes[6]. Besides these metabolic

A full list of affiliations appears at the end of the paper. ✉e-mail: wanghy@nicemice.cn; chenshuai@nju.edu.cn

alterations, the obese heart displays characteristics of impaired $Ca^{2+}$ homeostasis in cardiomyocytes, which can also cause cardiac dysfunction and contribute to the pathogenesis of obesity cardiomyopathy[4,7]. It is currently not clear whether and how the metabolic remodeling impacts on $Ca^{2+}$ homeostasis in the obese heart.

AS160 (also known as TBC1D4) is a component of insulin signaling, which is frequently mutated in Greenlandic and Canadian Inuits causing type 2 diabetes (T2D)[8,9]. Being a Rab-GTPase activating protein (RabGAP), AS160 regulates insulin-stimulated trafficking of both GLUT4 and CD36 in insulin-responsive cells/tissues[10,11]. Upon insulin stimulation, AS160 is phosphorylated by protein kinase B (PKB, also known as Akt) and consequently become inactive, which allows downstream Rabs to be converted to their GTP-loaded active form[10]. GTP-loaded Rabs such as Rab8a then promote translocation of GLUT4 and CD36 onto the plasma membrane to facilitate uptake of glucose and fatty acids into cells, respectively[11–13]. Besides its role in insulin-stimulated translocation of GLUT4 and CD36, AS160 is also involved in the regulation of lysosome-mediated degradation of GLUT4 after its internalization through endocytosis in multiple tissues including the heart[14]. In rats bearing a premature stop mutation, $AS160^{R693X}$ (a mutation homologous to human $AS160^{R684X}$ mutation in Inuit patients), deficiency of AS160 in skeletal muscle causes selective insulin resistance towards glucose metabolism through accelerating GLUT4 degradation via the lysosome, but simultaneously enhances fatty acid utilization through promoting CD36 translocation onto the plasma membrane[15]. A widely-accepted assumption is that high-fat diet (HFD) causes insulin resistance that consequently activates AS160 through inhibiting its phosphorylation. Mutation of a key insulin-responsive $Thr^{642}$ to a non-phosphorylatable alanine on AS160 inhibits insulin-stimulated GLUT4 trafficking and consequent glucose uptake in skeletal muscle in a knockin mouse model[16]. This $AS160^{T642A}$ mutation does not affect cardiac contractility in mice[17]. A recent study has shown that global deletion of AS160 abrogates cardiac glucose uptake and enhances myocardial damage after ischemia/reperfusion[18]. So far, it is not clear whether, and if so how, AS160 might respond to fatty acids to regulate cardiac metabolic remodeling and function in obesity.

In this study, we show that NIMA-related kinase 6 (NEK6) phosphorylates AS160 on its $Thr^{973}$ and thereby inhibits the GAP activity of AS160 in the heart in response to HFD and demonstrate that cardiac inactivation of AS160 causes metabolic remodeling in cardiomyocytes in a manner similar to HFD. Importantly, our study shows that AS160 inactivation in cardiomyocytes increases lysophosphatidylinositol metabolism and signaling that impairs $Ca^{2+}$ homeostasis and causes cardiac dysfunction. Targeting this NEK6-AS160 pathway alleviates obesity cardiomyopathy induced by HFD.

## Results

### Palmitic acid (PA)/HFD inhibits AS160 GAP activity in cardiomyocytes

AS160 and TBC1D1 are two related RabGAPs that are both regulated by insulin[10,19]. Analyses of their expression in primary cardiomyocytes and fibroblasts isolated from the heart revealed that AS160 is the dominant one in the cardiomyocytes while TBC1D1 is mainly expressed in the fibroblasts of the heart (Supplementary Fig. 1a). We subsequently focused on AS160 and investigated its potential roles in fatty acid-treated cardiomyocytes and in the heart of diet-induced obesity (DIO). Fluorophore-conjugated PA or oleic acid (OA) could be rapidly absorbed into rat H9C2 cardiomyocytes within minutes (Supplementary Fig. 1b). It has been shown that acute treatment with PA does not induce insulin resistance in H9C2 cardiomyocytes within 3 h[20]. Accordingly, acute treatments with PA or OA for 30 min did not alter the expression and $Thr^{642}$ phosphorylation of AS160 and its upstream kinase PKB in H9C2 cardiomyocytes (Fig. 1a, Supplementary Fig. 1c, d). The GAP activity of AS160 towards its bona fide substrate Rab8a was greatly decreased in PA-treated cardiomyocytes, and largely unaffected in OA-treated cardiomyocytes (Fig. 1b). Consistently, the GTP-loaded active Rab8a was significantly elevated in the cardiomyocytes acutely-treated with PA but not OA (Fig. 1c). Similar to the acute treatment, the chronic treatment with PA for 12 h also decreased the GAP activity of endogenous AS160 in neonatal rat ventricular cardiomyocytes (NRVCs) (Supplementary Fig. 1e). Moreover, PA treatment did not alter the expression of AS160 but inhibited its GAP activity in human induced pluripotent stem cell-derived cardiomyocytes (hiPSC-CMs) (Supplementary Fig. 1f, g). In agreement with these findings in cardiomyocytes, acute oral administration of PA, but not OA, decreased the GAP activity of AS160 without affecting its expression (Fig. 1d, e). In contrast, both PA and OA induced key genes in fatty acid transport and β-oxidation in the heart to similar levels when acutely administered into mice (Supplementary Fig. 1h). Thus, the effect of PA on the AS160 GAP activity was similar to that of insulin, the known regulator of AS160 through promoting its phosphorylation.

We then examined the regulation and activity of AS160 in the heart of DIO mice. Insulin expectedly increased the phosphorylation of AS160 and PKB in the heart of mice fed a normal chow diet (NCD) (Fig. 1f). In contrast, the insulin-induced phosphorylation of AS160 and PKB in the heart was moderately decreased in the heart of mice fed a HFD for 4 weeks (Fig. 1f). As expected, insulin markedly decreased the GAP activity of AS160 in the heart of mice fed with the NCD (Fig. 1g) in concomitance with an increased GTP-bound active Rab8a (Fig. 1h). Notably, the HFD feeding caused a significant decrease of the GAP activity of AS160 in mouse heart at the basal state and blunted the insulin-induced diminishment of the GAP activity of AS160 (Fig. 1g). In agreement, the HFD feeding increased the GTP-bound active Rab8a at the basal state but prevented its increase in response to insulin stimulation (Fig. 1h, Supplementary Fig. 1i). As expected, HFD did not alter protein expression of CD36 but markedly decreased the amounts of GLUT1 and GLUT4 proteins in mouse heart (Supplementary Fig. 1j).

We further investigated the activity of AS160 in the heart of obese rhesus macaques. The obese rhesus macaques developed cardiomyopathy with lower ejection fraction (EF) and fractional shortening (FS) as compared to the controls (Supplementary Fig. 1k, l). AS160 protein was normal, however its GAP activity was significantly decreased by nearly 50% in the heart of obese rhesus macaques (Fig. 1i, j). Both total protein of Rab8a and its GTP-bound active form were increased in the heart of obese rhesus macaques (Fig. 1k–m).

Taken together, these data demonstrate that PA/HFD inhibits the GAP activity of AS160 in cardiomyocytes, which is most likely not mediated by its $Thr^{642}$ phosphorylation.

### Inactivation of AS160 causes cardiac dysfunction and dilated cardiomyopathy

The inhibition of the AS160 GAP activity by PA/HFD intrigued us to investigate the possible consequences of impaired AS160 GAP function in the heart. To this end, we first utilized the $AS160^{R972K}$ mouse model in which the $AS160^{R972K}$ knockin mutation inactivates the GAP function of AS160 (numbering according to NP_001391600.1, previously known as $AS160^{R917K}$ according to NP_001074747.2)[14]. The inactivation of AS160-GAP activity did not affect the expression of TBC1D1 in the heart (Fig. 2a). Both male and female $AS160^{R972K}$ mice (2-6-month-old) displayed lower EF and FS (Fig. 2b, Supplementary Fig. 2b, c), suggesting that their cardiac function was impaired. The hearts of these mice exhibited dilation with the increased end-systolic left ventricle (LV) diameter and thinner LV anterior and posterior walls (Fig. 2b, Supplementary Fig. 2a–c). Insulin-stimulated phosphorylation of AS160 and PKB remained normal in the $AS160^{R972K}$ heart (Supplementary Fig. 2d). The $AS160^{R972K}$ mice displayed no apparent changes in the expression of cardiac remodeling markers in their hearts (Supplementary Fig. 2e). Similarly, a global AS160 knockout (KO) mouse model also developed dilated cardiomyopathy and cardiac dysfunction (Fig. 2c, d, Supplementary Fig. 2f).

https://doi.org/10.1038/s41467-024-54031-5

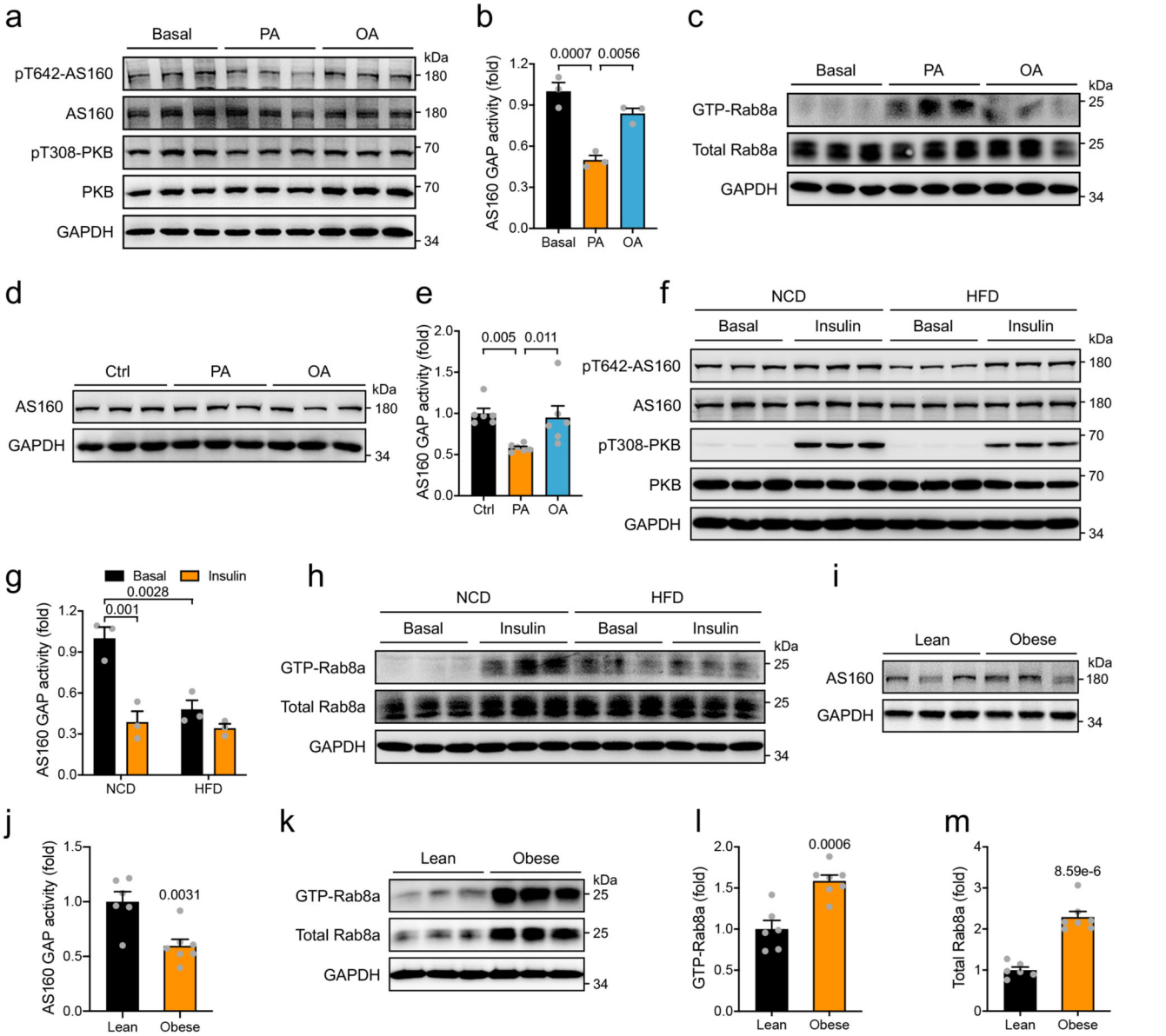


**Fig. 1 | Effects of PA/HFD on AS160 Thr$^{642}$-phosphorylation and GAP activity.** **a** Expression and phosphorylation of AS160 and PKB in PA- or OA-treated H9C2 cardiomyocytes. **b** GAP activity of endogenous AS160 in PA- or OA-treated H9C2 cardiomyocytes. $n = 3$ biological replicates. **c** Total and GTP-bound active Rab8a in PA- or OA-treated H9C2 cardiomyocytes. Expression (**d**) and GAP activity (**e**) of endogenous AS160 in the heart of mice administered with PA or OA for 3 h. $n = 6$. Ctrl, control. **f** Expression and phosphorylation of AS160 and PKB in the heart of mice fed normal chow diet (NCD) or HFD in response to insulin. **g** GAP activity of endogenous AS160 in the heart of mice fed NCD or HFD. $n = 3$. **h** Total and GTP-bound active Rab8a in the heart of mice fed NCD or HFD in response to insulin. Expression (**i**) and GAP activity (**j**) of endogenous AS160 in the heart of lean and obese monkeys (male, 5.6–26.9-year-old). $n = 6$ (Lean) and 7 (Obese). **k**–**m** Total and GTP-bound Rab8a in the heart of lean and obese monkeys (male, 5.6–26.9-year-old). $n = 6$ (Lean) and 7 (Obese). The data are given as the mean ± SEM. Numbers on the graphs represent $p$ values. Statistical analyses were carried out using one-way ANOVA for (**b**), (**e**), two-sided $t$-test for (**j**), (**l**), (**m**), and two-way ANOVA for (**g**). Source data are provided as a Source Data file.

Since the above-mentioned AS160$^{R972K}$ knockin and AS160 knockout mice are globally-modified models, it is possible that cardiac dysfunction in these models was due to some non-heart originated systemic signals. To investigate this possibility, we mated an AS160$^{f/f}$ mouse[14] with an αMHC-Cre mouse[21] to specifically delete AS160 in the heart after birth. AS160 protein was greatly decreased in the heart of AS160$^{f/f}$/αMHC-Cre mice (AS160 cardiac-specific knockout mice, abbreviated as AS160-cKO) but not in skeletal muscle (Supplementary Fig. 3a). Cardiac deletion of AS160 did not affect blood glucose and lipid levels in mice (Supplementary Fig. 3b–e). The proximal insulin signaling remained intact in the heart of AS160-cKO mice (Fig. 2e). However, both male and female AS160-cKO mice displayed impairment of cardiac function with lower EF and FS (Fig. 2f, Supplementary Fig. 3g, h). Their hearts developed dilation phenotype with the increased LV diameter under both systolic and diastolic conditions (Fig. 2f, Supplementary Fig. 3g, h). The LV anterior and posterior walls were thinner in the AS160-cKO mice than those in the AS160$^{f/f}$ littermate controls (Supplementary Fig. 3f–h). It has been reported that the ratio of the transmitral early and late peak filling rate (E/A), a measure of diastolic function, is decreased in diabetic cardiomyopathy[22]. Notably, the E/A was decreased in the AS160-cKO mice (Supplementary Fig. 3i, j). These data suggest that cardiac dysfunction caused by AS160 deficiency exhibits no dimorphic characteristics. Therefore, primary cardiomyocytes from both genders were used in the

https://doi.org/10.1038/s41467-024-54031-5

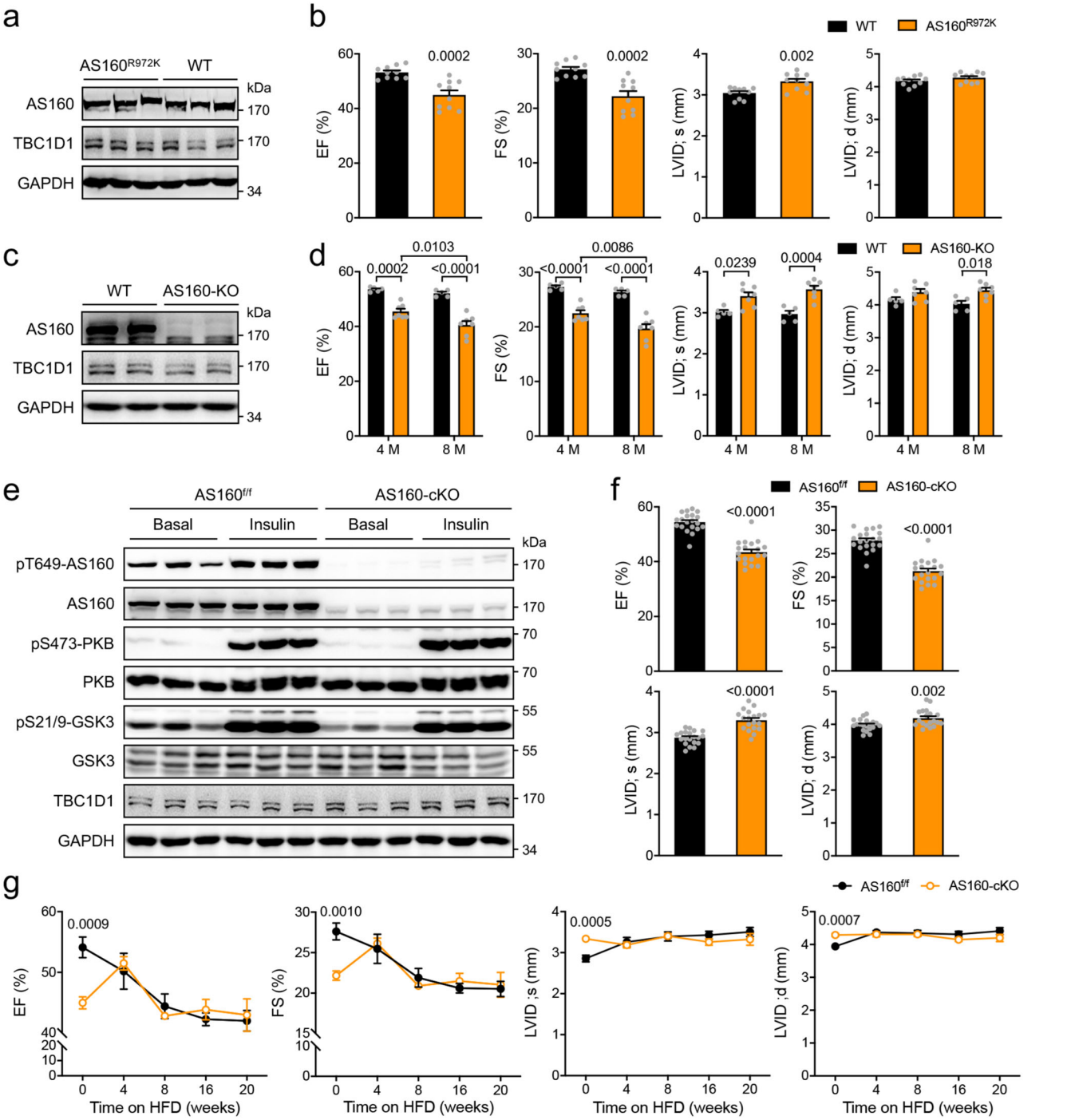


**Fig. 2 | Cardiac function in AS160 deficient or inactive mutant mice.** **a** Expression of AS160 and TBC1D1 in the heart of AS160$^{R972K}$ mice. **b** Cardiac function of AS160$^{R972K}$ mice. EF, FS, LVID;s and LVID;d were measured in male AS160$^{R972K}$ mice (6-month-old). $n = 10$. **c** Expression of AS160 and TBC1D1 in the heart of AS160-KO mice. **d** Cardiac function of AS160-KO mice. EF, FS, LVID;s and LVID;d were measured in male AS160-KO mice (4- and 8-month-old). $n = 5$ (WT) and 7 (AS160-KO). **e** Expression and phosphorylation of AS160, PKB, GSK3 and TBC1D1 in the heart of AS160-cKO mice. **f** Cardiac function of AS160-cKO mice. EF, FS, LVID;s and LVID;d were measured in male AS160-cKO mice (4-month-old). $n = 19$ (AS160-cKO) and 20 (AS160$^{f/f}$). **g** Cardiac function of AS160-cKO mice fed HFD. EF, FS, LVID;s and LVID;d were measured in male AS160-cKO mice that were fed HFD from the age of 5-month. $n = 6$. The data are given as the mean ± SEM. Numbers on the graphs represent $p$ values. Statistical analyses were carried out using two-way ANOVA for (**d**), and two-sided $t$-test for (**b**), (**f**), (**g**). Source data are provided as a Source Data file.

subsequent cellular analyses. The sizes of cardiomyocytes were increased in the AS160-cKO mice (Supplementary Fig. 3k). Again, no apparent changes in cardiac remodeling marker gene expression occurred in the heart of AS160-cKO mice (Supplementary Fig. 3l). It has recently been reported that whole-body deletion of AS160 increases expression of matrix metalloproteinases and triggers cardiac endoplasmic reticulumn (ER) stress response[18]. In contrast, cardiomyocyte-specific deletion of AS160 did not induce such changes in the heart (Supplementary Fig. 3m–o).

We then subjected the AS160-cKO and AS160$^{f/f}$ mice to HFD feeding. Cardiac function of the AS160$^{f/f}$ control mice was progressively decreased within the first 8 weeks on HFD and became

stabilized afterwards. Cardiac contractility of the AS160-cKO mice was lower than that of the AS160$^{f/f}$ controls before HFD feeding. Interestingly, cardiac function of the AS160-cKO mice was enhanced at 4 weeks after HFD, and then declined in a manner similar to that of the AS160$^{f/f}$ controls (Fig. 2g). Both systolic and diastolic LV diameters were increased in the WT mice, but not in the AS160-cKO mice, after HFD feeding (Fig. 2g). Given that HFD/PA could rapidly inactivate the GAP of AS160 in the heart, these data suggest that HFD impairs cardiac function likely through AS160 at least in the early phase.

Together, these data demonstrate that AS160 plays a role in heart function. Its deficiency in cardiomyocytes impairs cardiac function and causes dilated cardiomyopathy through a heart-autonomous mechanism.

### Cardiac inactivation of AS160 does not alter energy levels in the heart

Since AS160 is known as a metabolic regulator, we wondered whether its cardiac deletion might cause an energy deficit that leads to cardiac dysfunction. A recent study has shown that GLUT4 protein and insulin-stimulated glucose uptake are decreased in the heart of whole-body AS160 knockout mice[18]. Similarly, GLUT4 was markedly decreased in the heart of global or cardiac-specific AS160 inactive mutant mice while its mRNA levels were unchanged (Supplementary Fig. 4a–d). Insulin markedly increased GLUT4 levels on the cell surface in the WT cardiomyocytes (Supplementary Fig. 4e, f). In contrast, the insulin-stimulated GLUT4 translocation was greatly inhibited in the AS160 deficient cardiomyocytes (Supplementary Fig. 4e, f). Previous studies show that cardiac deletion of GLUT4 resulted in upregulation of GLUT1 as a compensatory response[23]. We did not observe such a compensatory response in the heart of AS160 inactive mutant mice. Instead, we found that both *glut1* mRNA and GLUT1 protein were markedly decreased in the heart of these AS160 inactive mutant mice (Supplementary Fig. 4a–d). As a consequence of diminished GLUT1 and GLUT4 proteins, both basal and insulin-stimulated glucose uptake were significantly decreased, and the insulin responsiveness was blunted in the AS160 deficient primary cardiomyocytes as compared to the wild-type cells (Supplementary Fig. 4g). Moreover, in vivo glucose uptake into the heart was lower in the AS160-cKO mice than in the AS160$^{f/f}$ littermate controls (Supplementary Fig. 4h). Cardiomyocyte-specific deletion of AS160 affected neither expression of key genes in glucose metabolism in skeletal muscle, liver and adipose tissue nor the clearance of blood glucose in the oral glucose tolerance test (Supplementary Fig. 5a–d). The inhibition of cardiac glucose uptake led us to suspect an energy deficit in the AS160-deficient heart. In fact, the ATP levels were moderately upregulated in the AS160-deficient heart (Supplementary Fig. 4i).

Fatty acids (FAs) are another important class of fuel substrates in the heart, and their uptake into cardiomyocytes is mainly mediated by the fatty acid translocase CD36[24,25]. CD36 protein level was normal in the AS160-deficient heart (Supplementary Fig. 4e, f). CD36 undergoes translocation from the intracellular storage sites onto the cell surface of cardiomyocytes in response to insulin stimulation, which is governed by the AS160-Rab8a axis[11]. As expected, insulin markedly increased cell surface CD36 in the WT cardiomyocytes (Supplementary Fig. 4e, f, Supplementary Fig. 4j–m). Importantly, cell surface CD36 levels were higher in the AS160 deficient cardiomyocytes than in the WT cells under both basal and insulin-stimulated conditions (Supplementary Fig. 4e, f, Supplementary Fig. 4j–m). FATP4 is another FA transporter and its protein expression is increased in skeletal muscle of AS160 knockout mice[26]. However, total FATP4 expression was not altered in the heart of AS160-cKO mice (Supplementary Fig. 4n, o). Similar to CD36, FATP4 can also undergo translocation onto the cell surface in response to insulin[27]. Of note, AS160 deficiency enhanced insulin-stimulated FATP4 translocation in primary cardiomyocytes (Supplementary Fig. 4p, q). These data suggest that FA uptake might be upregulated due to the enhanced translocation of multiple FA transporters including CD36 and FATP4 in AS160 deficient heart. Indeed, insulin-stimulated FA uptake was higher in the AS160 deficient cardiomyocytes than in the WT cells (Supplementary Fig. 4r, s). The insulin response for FA uptake was also higher in the AS160 deficient cardiomyocytes than in the wild-type cells. Furthermore, in vivo FA uptake into the heart was higher in the AS160-cKO mice than in the AS160$^{f/f}$ littermate controls (Supplementary Fig. 4t). In agreement with the upregulation of FA uptake, FA oxidation was increased in the AS160 deficient heart in an O2K assay when PC/malate were used as fuel substrates (Supplementary Fig. 4u). The enhanced cardiac FA utilization in the AS160-cKO mice might contribute to the transient improvement of their cardiac function within the first 4 weeks on HFD (Fig. 2g). We examined whether cardiomyocyte-specific deletion of AS160 might impact on lipid metabolism in peripheral tissues, and found that it did not affect expression of key genes in lipid metabolism in skeletal muscle, liver and adipose tissue (Supplementary Fig. 5a–c).

Together, these data show that AS160 is a regulator of metabolic flexibility in the heart. Its inactivation inhibits glucose utilization and simultaneously enhances FA metabolism for maintenance of cardiac energy levels.

### AS160 deficiency impairs cardiomyocyte $Ca^{2+}$ homeostasis

$Ca^{2+}$ is a critical regulator of cardiac function, and defects in its shuttling between the cytosol and sarcoplasmic reticulum (SR) lead to cardiac dysfunction. Cardiac expression of key regulators of $Ca^{2+}$ homeostasis, including LTCC, NCX, SERCA2a and RYR2, displayed no difference between the AS160-cKO and AS160$^{f/f}$ mice at both mRNA and protein levels (Supplementary Fig. 6a–c). The L-type $Ca^{2+}$ current was not altered in primary cardiomyocytes isolated from the AS160-cKO mice (Supplementary Fig. 6d, e). We then employed a confocal microscope to measure field stimulation-induced $Ca^{2+}$ transients in primary cardiomyocytes using a fluo-4 probe. The amplitude of $Ca^{2+}$ transients, a measure of cytosolic $Ca^{2+}$, was significantly lower in primary cardiomyocytes isolated from the AS160-cKO mice than in the AS160$^{f/f}$ controls in concomitance with increased full duration at half maximum (FDHM) and time constant Tau (Fig. 3a, b, Supplementary Fig. 6f). Similarly, the $Ca^{2+}$ transients were depressed with concomitant increases of FDHM and Tau in NRVCs when AS160 was transiently depleted via small interfering RNA (siRNA) (Fig. 3c, d). Protein expression and phosphorylation of SERCA2a were comparable between the AS160-cKO mice and AS160$^{f/f}$ littermates (Supplementary Fig. 6b). Protein expression of phospholamban, a regulator of SERCA2a, was also unaltered in the AS160-cKO heart (Supplementary Fig. 6g). We then measured ATPase and $Ca^{2+}$ transport activities of SERCA2a in microsomes isolated from the AS160-cKO and AS160$^{f/f}$ mice, and found no difference between the two genotypes (Supplementary Fig. 6h, i). RYR2-mediated $Ca^{2+}$ leakage from the SR results in $Ca^{2+}$ sparks that are elementary units of $Ca^{2+}$ release[28]. Interestingly, more $Ca^{2+}$ sparks were found in cardiomyocytes from the AS160-cKO mice than in AS160$^{f/f}$ control cells (Fig. 3e, f, Supplementary Fig. 6j, k), suggesting that RYR2-mediated $Ca^{2+}$ leakage from the SR was increased in the AS160-cKO heart. In agreement, RYR2 phosphorylation that enhances its activity was significantly increased in the AS160-cKO heart (Fig. 3g, h). These data suggest that the prolonged clearance of cytosolic $Ca^{2+}$ in AS160 deficient heart is most likely due to RYR2-mediated SR $Ca^{2+}$ leakage rather than SERCA2a-dependent SR $Ca^{2+}$ re-uptake. Furthermore, SR $Ca^{2+}$ load was significantly lower in cardiomyocytes from the AS160-cKO mice at the age of 6 and 12 months than in AS160$^{f/f}$ control cells (Fig. 3i, j, Supplementary Fig. 6l, m), which is in agreement with increased SR $Ca^{2+}$ leakage.

https://doi.org/10.1038/s41467-024-54031-5

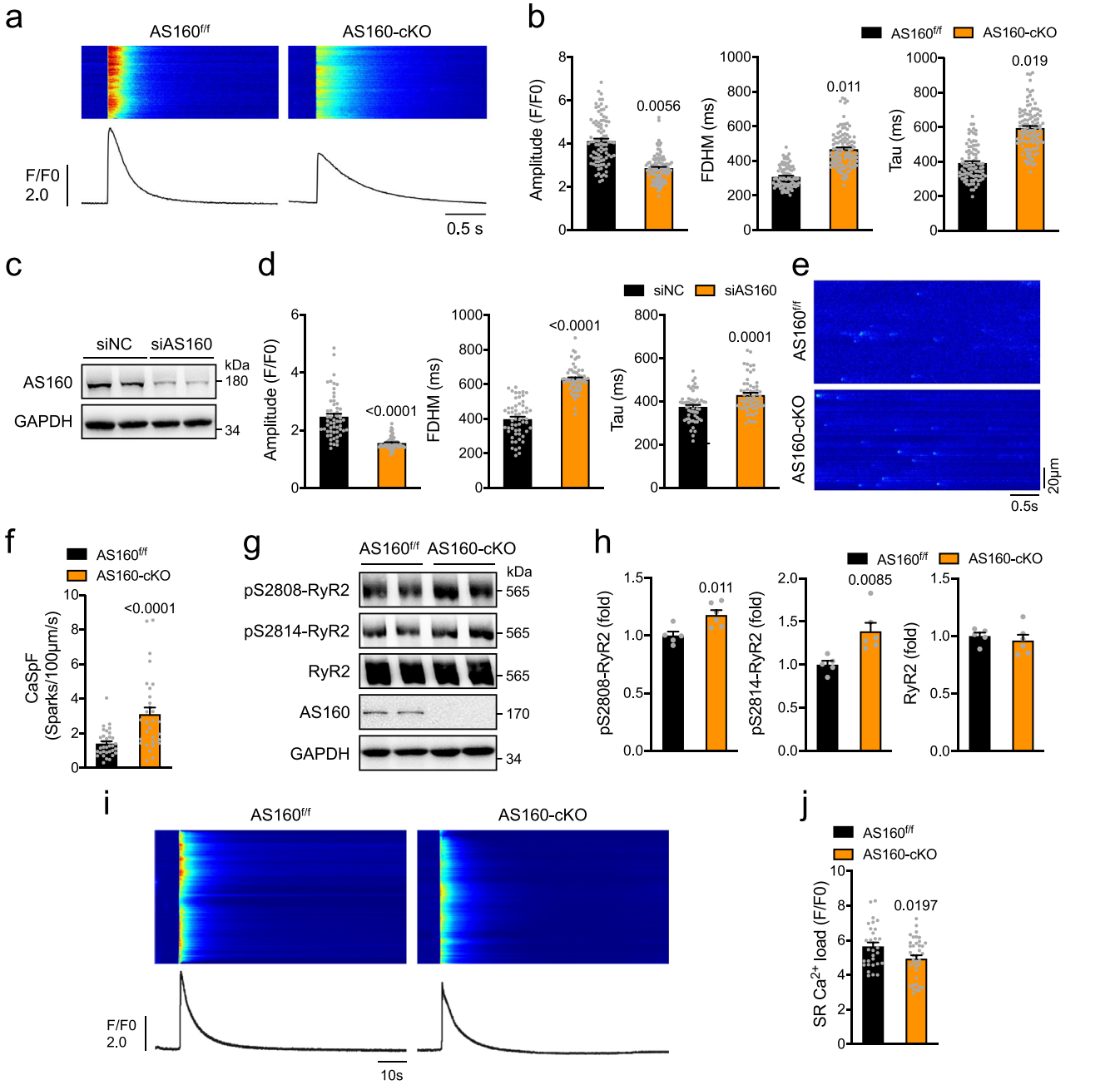


**Fig. 3 | $Ca^{2+}$ homeostasis in AS160 deficient cardiomyocytes. a**, **b** $Ca^{2+}$ transients in primary cardiomyocytes isolated from the $AS160^{f/f}$ and AS160-cKO mice (2-month-old, female) upon field stimulation. **a** Representative $Ca^{2+}$ transient images and curves. **b** Amplitude, FDHM and Tau of $Ca^{2+}$ transients. $AS160^{f/f}$: 91 cells from 3 mice. AS160-cKO: 106 cells from 4 mice. **c** AS160 protein expression in AS160-knockdown neonatal rat cardiomyocytes. **d** $Ca^{2+}$ transients in AS160-knockdown neonatal rat cardiomyocytes upon field stimulation. Amplitude, FDHM and Tau of $Ca^{2+}$ transients were measured from 57 (siNC) and 59 (siAS160) cells. **e**, **f** $Ca^{2+}$ sparks in primary cardiomyocytes isolated from the $AS160^{f/f}$ and AS160-cKO (2-month-old, male). **e** Representative images of $Ca^{2+}$ sparks. **f** Quantification of $Ca^{2+}$ spark frequency. 34 cells from 4 $AS160^{f/f}$ mice and 30 cells from 3 AS160-cKO mice were measured. **g**, **h** Expression and phosphorylation of RYR2 in the heart of female AS160-cKO and $AS160^{f/f}$ mice (3-month-old). **g** Representative blots. **h** Quantification of RYR2 protein and phosphorylation levels. $n = 5$ ($AS160^{f/f}$) and 6 (AS160-cKO). **i**, **j** SR $Ca^{2+}$ load in primary cardiomyocytes isolated from the $AS160^{f/f}$ and AS160-cKO mice (6-month-old, female). **i** Representative SR $Ca^{2+}$ load images and curves. **j** Quantification of SR $Ca^{2+}$ load. 30 cells from 5 $AS160^{f/f}$ mice and 38 cells from 5 AS160-cKO mice were measured. The data are given as the mean ± SEM. Numbers on the graphs represent *p* values. Statistical analyses were carried out using two-sided nested *t*-test for (**b**), (**f**), (**j**), and two-sided *t*-test for (**d**), (**h**). Source data are provided as a Source Data file.

Taken together, AS160 deficiency impairs $Ca^{2+}$ homeostasis in cardiomyocytes probably through RYR2-mediated SR $Ca^{2+}$ leakage.

### AS160 deficiency-elicited lysophosphatidylinositol (LPI) impairs $Ca^{2+}$ homeostasis and cardiomyocyte contractility

To gain more insights how AS160 deficiency impairs cardiac $Ca^{2+}$ homeostasis, we performed a lipidomic study in the heart. In total, 584 lipid species in 29 classes of lipids were identified in the heart via mass-spectrometry, among which 130 lipid species were altered in the AS160-cKO heart (Fig. 4a). Ceramides and sphingolipids did not differ in the heart between the AS160-cKO and $AS160^{f/f}$ mice (Supplementary Fig. 7a), suggesting no apparent lipotoxicity in the AS160-cKO heart during the experimental period. The most pronounced changes were observed for glycerophospholipids including lysophosphatidic acid

https://doi.org/10.1038/s41467-024-54031-5

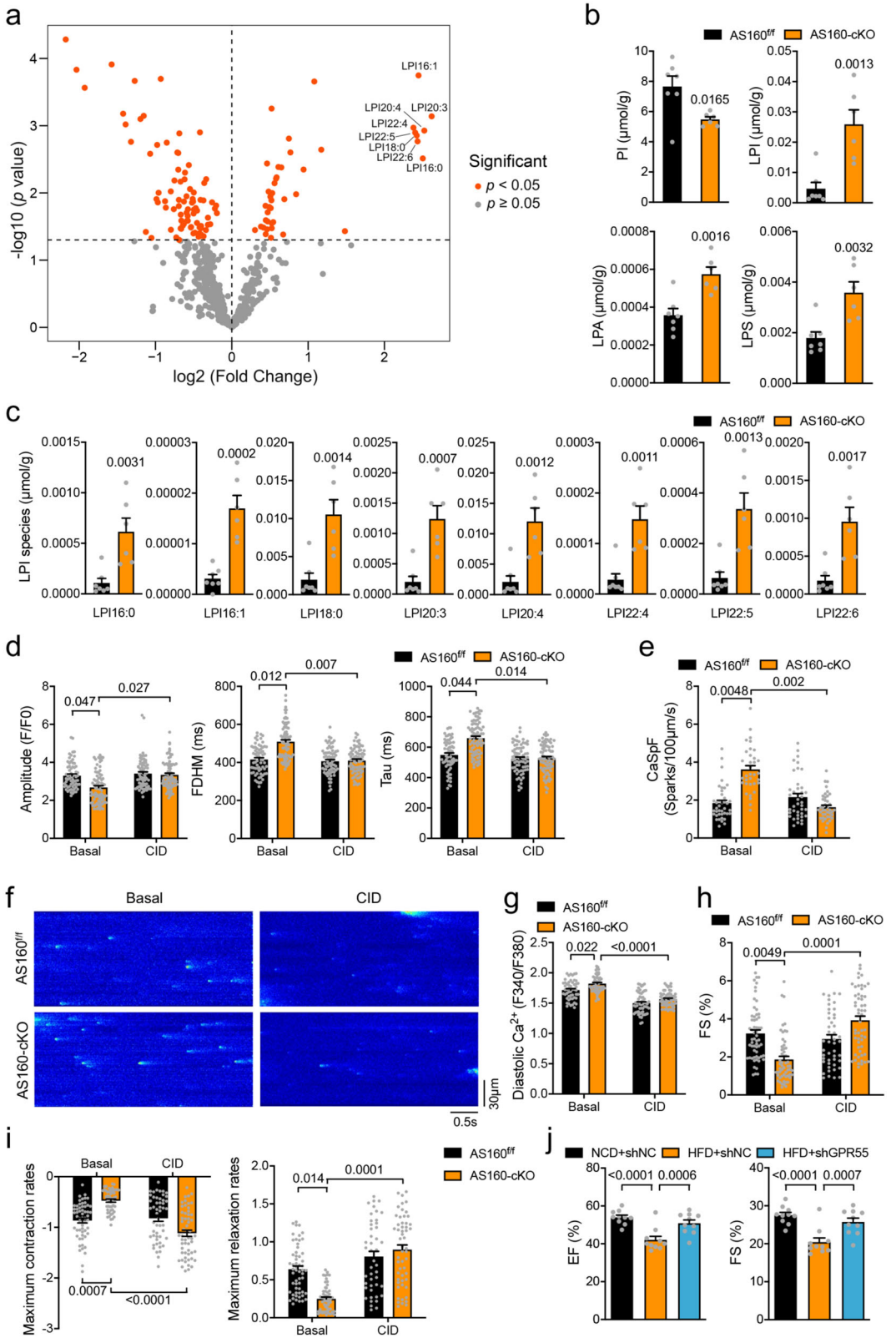


(LPA), lysophosphatidylinositol (LPI), lysophosphatidylserine (LPS) and phosphatidylinositol (PI). Total LPA, LPI and LPS were markedly increased, whereas total PI was significantly decreased, in the AS160-cKO heart (Fig. 4b). All eight LPI species detected in the heart through mass-spectrometry were elevated in the AS160-cKO mice (Fig. 4c). It has been shown that LPI increases cytosolic $Ca^{2+}$ through binding to its receptor GPR55[29]. In agreement, treatment with LPI depressed $Ca^{2+}$ transients and increased FDHM and Tau to extents similar to knockdown of AS160 in NRVCs (Supplementary Fig. 7b). CID16020046 (CID), a GPR55 inhibitor[30], prevented depression of $Ca^{2+}$ transients and restored FDHM and Tau in cardiomyocytes from the AS160-cKO mice as well as the $AS160^{R972K}$ mice (Fig. 4d, Supplementary Fig. 7c). Moreover, CID treatment blocked the increase of $Ca^{2+}$ sparks in AS160-cKO cardiomyocytes (Fig. 4e, f). Diastolic $Ca^{2+}$ was significantly increased in

**Fig. 4 | LPI metabolism and signaling in AS160 deficient cardiomyocytes.** **a** Volcano plot of fold-change of lipid metabolites in the heart of the AS160$^{f/f}$ and AS160-cKO mice (male, 8-week-old). Fold-change was given as the ratio of AS160-cKO to AS160$^{f/f}$. $n = 6$ (AS160-cKO) and 7 (AS160$^{f/f}$). **b** Levels of total PI, LPI, LPA and LPS in the heart of the AS160$^{f/f}$ and AS160-cKO mice (male, 8-week-old). $n = 6$ (AS160-cKO) and 7 (AS160$^{f/f}$). **c** Levels of LPI species in the heart of the AS160$^{f/f}$ and AS160-cKO mice (male, 8-week-old). $n = 6$ (AS160-cKO) and 7 (AS160$^{f/f}$). **d** $Ca^{2+}$ transients in primary cardiomyocytes isolated from the AS160$^{f/f}$ and AS160-cKO mice (6-month-old, female) upon treatment with the GPR55 inhibitor CID16020046 (CID). AS160$^{f/f}$: 65 (Basal) and 70 (CID) cells from 4 mice. AS160-cKO: 79 (Basal) and 75 (CID) cells from 4 mice. **e**, **f** $Ca^{2+}$ sparks in primary cardiomyocytes isolated from the AS160$^{f/f}$ and AS160-cKO mice (3-month-old, female) upon CID treatment. AS160$^{f/f}$: 40 (Basal) and 40 (CID) cells from 3 mice. AS160-cKO: 34 (Basal) and 41 (CID) cells from 3 mice. **e** quantification of $Ca^{2+}$ spark frequency. **f** Representative images of $Ca^{2+}$ sparks. **g** Diastolic $Ca^{2+}$ in cardiomyocytes from the AS160$^{f/f}$ and AS160-cKO mice (4-month-old, male). AS160$^{f/f}$: 52 (Basal) and 57 (CID) cells from 5 mice. AS160-cKO: 54 (Basal) and 58 (CID) cells from 5 mice. Contractility in primary cardiomyocytes isolated from the AS160$^{f/f}$ and AS160-cKO mice (4-month-old, male) upon CID treatment. FS (**h**), and maximum contraction rates and maximum relaxation rates (**i**) were determined via the IonOptix system. For FS, AS160$^{f/f}$: 59 (Basal) and 47 (CID) cells from 5 mice, AS160-cKO: 56 (Basal) and 54 (CID) cells from 5 mice. For maximum contraction rates, AS160$^{f/f}$: 57 (Basal) and 51 (CID) cells from 5 mice, AS160-cKO: 49 (Basal) and 56 (CID) cells from 5 mice. For maximum relaxation rates, AS160$^{f/f}$: 57 (Basal) and 45 (CID) cells from 5 mice, AS160-cKO: 55 (Basal) and 54 (CID) cells from 5 mice. **j** Cardiac function in AAV9-shNC or AAV9-shGPR55 administered male mice that were subjected to HFD for 6 weeks. $n = 10$. The data are given as the mean ± SEM. Numbers on the graphs represent $p$ values. Statistical analyses were carried out using two-sided $t$-test for (**a**), (**b**), (**c**), nested two-way ANOVA for (**d**, **e**), (**g**–**i**), and one-way ANOVA for (**j**). Source data are provided as a Source Data file.

AS160-cKO cardiomyocytes and this increase was eliminated upon treatment with the GPR55 inhibitor CID (Fig. 4g). Similarly, CID blocked the elevation of cytosolic $Ca^{2+}$ in NRVCs induced by knockdown of AS160 (Supplementary Fig. 7d).

We next sought to find out whether the LPI-elicited elevation of diastolic $Ca^{2+}$ and depression of $Ca^{2+}$ transient might impact on cardiomyocyte contractility in the AS160-cKO mice. To this end, we subjected primary cardiomyocytes to field stimulation and measured their contractility in concomitance with $Ca^{2+}$ transient via an IonOptix system. Pacing-induced $Ca^{2+}$ transient amplitude was significantly decreased in AS160 deficient cardiomyocytes, and this decrease was blocked by CID treatment (Supplementary Fig. 7e). Sarcomere shortening as well as maximum contraction and relaxation rates were significantly decreased in AS160 deficient cardiomyocytes (Fig. 4h, i), suggesting that their contractility was reduced. Notably, CID treatment prevented the decreases of sarcomere shortening as well as maximum contraction and relaxation rates in AS160-cKO cardiomyocytes (Fig. 4h, i).

These findings prompted us to investigate whether down-regulation of GPR55 might alleviate cardiac dysfunction in DIO mice in which AS160 GAP activity is inhibited. We knocked down GPR55 in the heart via an AAV-mediated expression of short-hairpin RNA (shRNA) targeting GPR55 (Supplementary Fig. 8a–c). Knockdown of GPR55 affected neither the development of obesity induced by HFD nor the elevation of blood glucose (Supplementary Fig. 8d, e). Notably, knockdown of GPR55 impeded the HFD-induced decline of cardiac function in mice (Fig. 4j).

Together, these data show that AS160 deficiency enhances LPI production and signaling to elevate cytosolic $Ca^{2+}$ in cardiomyocytes. The enhanced LPI signaling accounts for the impaired contractility in AS160 deficient cardiomyocytes.

## AS160 and its downstream Rab8a regulate LPI metabolism in the cardiomyocytes

We next sought to find out how AS160 regulates LPI metabolism in cardiomyocytes. LPI in cells exists as sn-1 or sn-2 lysophospholipids, which are produced by two distinct phospholipases, cytosolic PLA2 (cPLA2) and intracellular phospholipase A1 (DDHD Domain Containing 1, DDHD1), through removal of the acyl group from PI at sn-2 or sn-1 position, respectively. LPI can be deacylated into glycerophosphoinositol by lysophospholipases, such as ABHD6 and lyso-PLA, and reacylated into PI via 1-acylglycerol-3-phosphate acyltransferase 8 (AGPAT8) or Membrane-bound O-acyltransferase 7 (MBOAT7) (Fig. 5a). RNA or protein levels of these LPI-metabolic enzymes in the heart exhibited no difference between the AS160-cKO mice and AS160$^{f/f}$ controls (Supplementary Fig. 9a, b). We then examined whether AS160 might regulate some of these enzymes through direct interaction. To this end, we co-expressed GFP-AS160 with Flag-tagged DDHD1, cPLA2, ABHD6, AGPAT8 and MBOAT7 in HEK293 cells, and measured their interaction via co-immunoprecipitation (co-IP). Notably, this assay revealed that GFP-AS160 interacted with Flag-tagged DDHD1 and cPLA2, two enzymes for LPI synthesis (Fig. 5b, d), but not with Flag-tagged ABHD6, AGPAT8 and MBOAT7 (Supplementary Fig. 9c–e). Reciprocal co-IP further showed that GFP-tagged DDHD1 and cPLA2 interacted with Flag-AS160 when co-expressed in cells (Fig. 5c, e). Endogenous DDHD1 and cPLA2 could be detected in the immunoprecipitates of Flag-AS160 (Fig. 5f). Moreover, endogenous AS160 was co-immunoprecipitated with endogenous DDHD1 (Fig. 5g). Protein expression of DDHD1 and cPLA2 did not change in the heart of DIO mice (Supplementary Fig. 9f, g). Interestingly, more mCherry-DDHD1 was co-localized with the ER marker GFP-VABP2 in response to PA treatment (Supplementary Fig. 9h, i), suggesting that PA might promote DDHD1 association with the ER that is a major site for LPI synthesis.

Rab8a is the well-known downstream target of AS160, whose active GTP-bound form was markedly increased in the AS160-cKO heart (Fig. 5h, i). Notably, Rab8a interacted with both cPLA2 and DDHD1 in the co-IP assay although it might exhibit a higher affinity towards DDHD1 than towards cPLA2 (Fig. 5j). Moreover, endogenous Rab8a was co-immunoprecipitated with endogenous DDHD1 (Fig. 5g). A GTP-bound Rab8a$^{Q67L}$ mutant, but not a GDP-bound Rab8a$^{T22N}$ mutant, displayed the ability to interact with GFP-tagged DDHD1 and cPLA2 in the co-IP assay (Fig. 5k, l). DDHD1 accounts for the production of LPI20:4 that is an endogenous ligand of GPR55[31]. We then examined whether Rab8a could regulate DDHD1 enzymatic activity in vitro. Notably, a GTP-loaded Rab8a increased the enzymatic activity of a recombinant DDHD1 to convert PI to sn-2 LPI20:4 (Fig. 5m). Knockdown of Rab8a prevented elevation of cytosolic $Ca^{2+}$ induced by depletion of AS160 in cardiomyocytes (Supplementary Fig. 9j).

Together, these data show that the AS160-Rab8a signaling module regulates DDHD1 through direct interaction for the production of LPI20:4, the endogenous ligand of GPR55.

## NEK6 phosphorylates Thr$^{973/976}$ on AS160 to inactivate its GAP function

Next, we sought to find out how HFD/PA inactivates the GAP function of AS160. HFD/PA might elicit some post-translational modification of AS160 thus inactivating its GAP function. We subjected AS160 to prediction of phosphorylation sites using the Scansite (https://scansite4.mit.edu) with medium stringency and noted that Thr$^{973}$ was predicted as a potential NEK6 phosphorylation site (Supplementary Fig. 10a). Given the location of Thr$^{973}$ and Thr$^{976}$ that are adjacent to the active site Arg$^{972}$ of the GAP of AS160, we focused on the potential phosphorylation of AS160-Thr$^{973/976}$ by NEK6 and examined their possible role in regulation of HFD/PA-elicited inactivation of AS160. Indeed, a maltose binding protein (MBP)-tagged recombinant AS160$^{S763\text{-}P1290}$ protein could be phosphorylated by a purified Flag-NEK6 in vitro (Fig. 6a). Furthermore, an AS160-Thr$^{973/976}$ containing peptide

https://doi.org/10.1038/s41467-024-54031-5

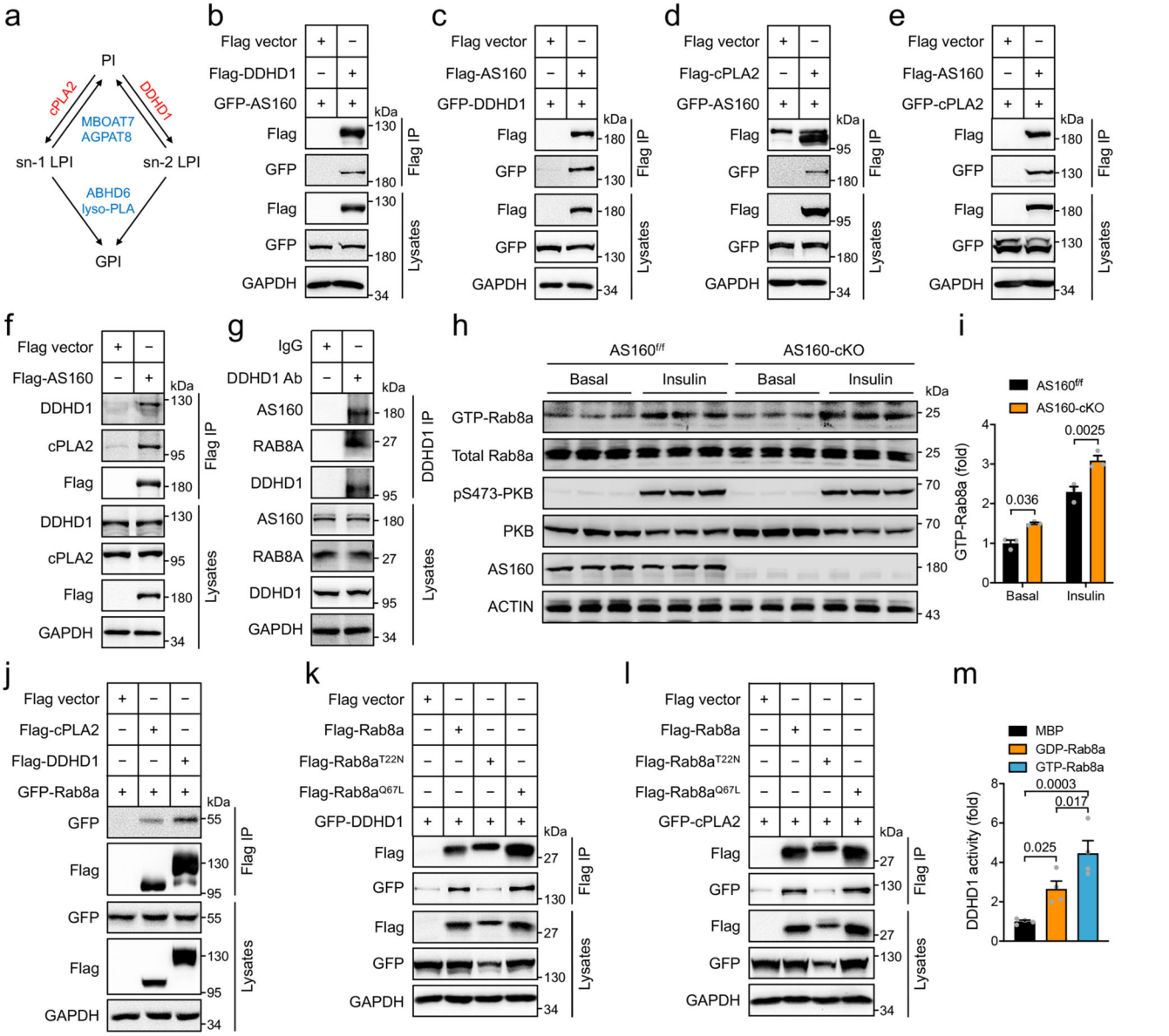


**Fig. 5 | Regulation of LPI metabolism by AS160 and Rab8a. a** Schematic illustration of LPI metabolic pathway. **b** Co-immunoprecipitation of GFP-AS160 with Flag-DDHD1. Flag-DDHD1 was co-expressed with GFP-AS160 in HEK293 cells, and immunoprecipitated from cell lysates using the Flag antibody. **c** Co-immunoprecipitation of GFP-DDHD1 with Flag-AS160. Flag-AS160 was co-expressed with GFP-DDHD1 in HEK293 cells, and immunoprecipitated from cell lysates using the Flag antibody. **d** Co-immunoprecipitation of GFP-AS160 with Flag-cPLA2. Flag-cPLA2 was co-expressed with GFP-AS160 in HEK293 cells, and immunoprecipitated from cell lysates using the Flag antibody. **e** Co-immunoprecipitation of GFP-cPLA2 with Flag-AS160. Flag-AS160 was co-expressed with GFP-cPLA2 in HEK293 cells, and immunoprecipitated from cell lysates using the Flag antibody. **f** Co-immunoprecipitation of endogenous DDHD1 and cPLA2 with Flag-AS160. Flag-AS160 was expressed in HEK293 cells, and immunoprecipitated from cell lysates using the Flag antibody. **g** Co-immunoprecipitation of endogenous AS160 and Rab8a with endogenous DDHD1 in H9C2 cardiomyocytes. **h**, **i** GTP-bound active Rab8a in AS160$^{f/f}$ and AS160-cKO cardiomyocytes in response to insulin. **h** Immunoblots. **i** Rab8a activation in which GTP-Rab8a was normalized with total Rab8a. $n = 3$ biological replicates. **j** Co-immunoprecipitation of GFP-Rab8a with Flag-DDHD1 or Flag-cPLA2. Flag-DDHD1 or Flag-cPLA2 was co-expressed with GFP-Rab8a in HEK293 cells, and immunoprecipitated from cell lysates using the Flag antibody. **k**, **l** Co-immunoprecipitation of GFP-DDHD1 or GFP-cPLA2 with Flag-tagged Rab8a WT or mutants. Flag-tagged Rab8a WT or mutants were co-expressed with GFP-DDHD1 (**k**) or GFP-cPLA2 (**l**) in HEK293 cells, and immunoprecipitated from cell lysates using the Flag antibody. **m** In vitro DDHD1 activity in the presence of GDP- or GTP-loaded Rab8a. $n = 4$ biological replicates. The data are given as the mean ± SEM. Numbers on the graphs represent $p$ values. Statistical analyses were carried out using two-way ANOVA for (**i**), and one-way ANOVA for (**m**). Source data are provided as a Source Data file.

(LVDLGRtFPtHP, Thr$^{973/976}$ shown in lower case) was phosphorylated by the purified Flag-NEK6 in vitro (Supplementary Fig. 10b). We mutated Thr$^{973}$ or Thr$^{976}$ or both to non-phosphorylatable alanine on recombinant MBP-AS160$^{S763\text{-}P1290}$, and found that the purified Flag-NEK6 could no longer phosphorylate the protein (Fig. 6a). Similarly, the purified Flag-NEK6 could phosphorylate neither an AS160-Thr$^{973}$Ala mutant peptide (LVDLGRaFPTHP, Ala$^{973}$ shown in lower case) nor an AS160-Thr$^{976}$Ala mutant peptide (LVDLGRTFPaHP, Ala$^{976}$ shown in lower case) (Supplementary Fig. 10c). When Flag-AS160 and GFP-NEK6 were co-expressed in HEK293 cells, the two proteins exhibited interaction in a co-IP assay (Supplementary Fig. 10d, e). Interestingly, PA treatment increased the kinase activity of Flag-NEK6 (Fig. 6b, c). We then raised a site-specific antibody recognizing phosphorylated Thr$^{973}$ on AS160. In the presence of GFP-NEK6, PA increased the phosphorylation of Thr$^{973}$ on Flag-AS160 (Fig. 6d). The AS160$^{T973A}$ mutation prevented, while the AS160$^{T976A}$ mutation decreased, the PA-induced Thr$^{973}$ phosphorylation

https://doi.org/10.1038/s41467-024-54031-5

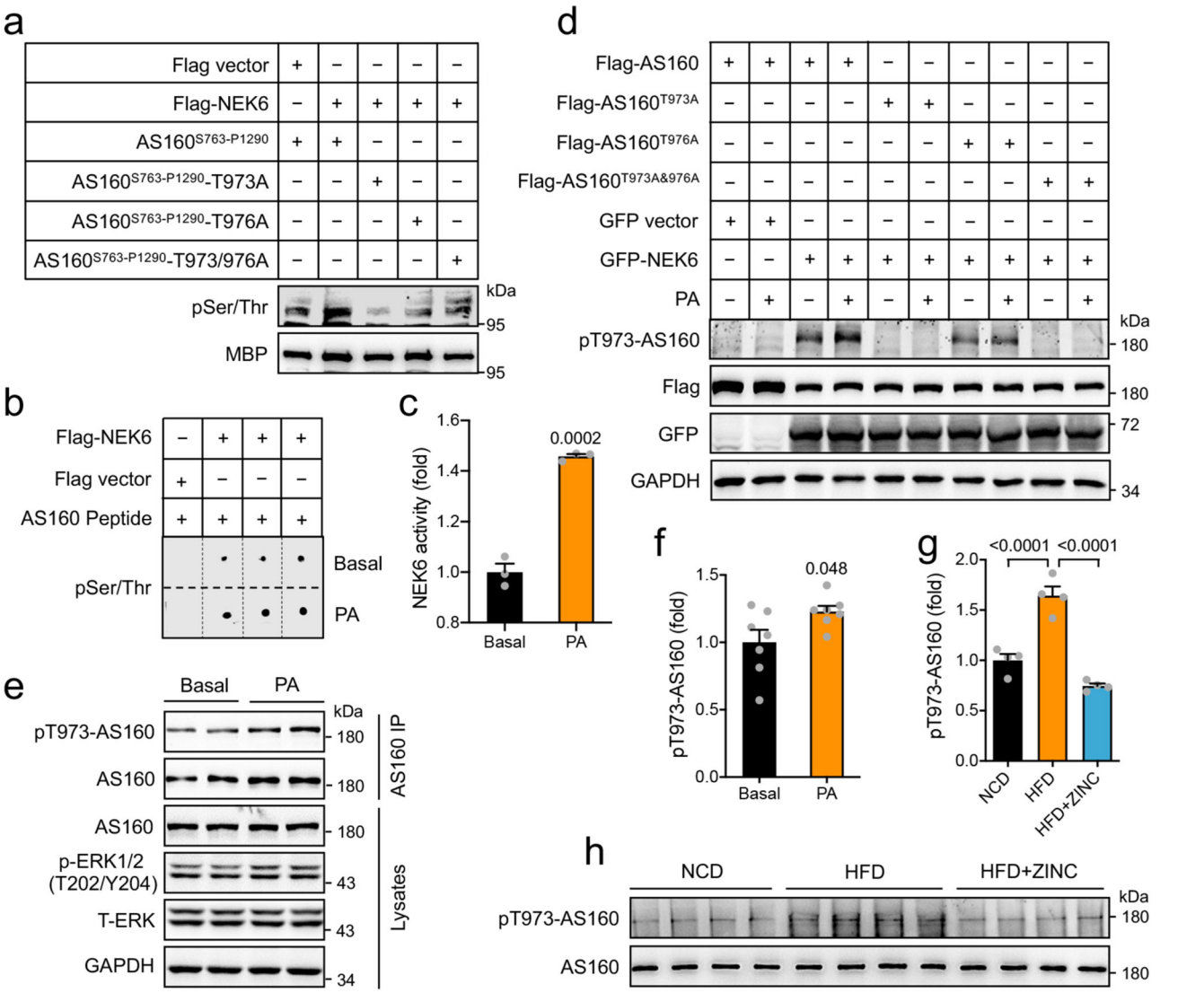


**Fig. 6 | Phosphorylation of AS160 by NEK6 in response to PA. a** In vitro phosphorylation of recombinant MBP-AS160$^{S763\text{-}P1290}$ WT and mutant proteins by a purified Flag-NEK6. Phosphorylation of MBP-AS160$^{S763\text{-}P1290}$ WT and mutant proteins was detected using a pSer/Thr antibody. **b**, **c** NEK6 activity in response to PA. Flag-NEK6 was immunoprecipitated from HEK293 cells that were stimulated with or without PA, and assayed for its kinase activity using AS160-Nektide (LVDLGRtFPtHP, Thr$^{973/976}$ shown in lower case) as a substrate. **b** Dot blots. **c** NEK6 activity. $n = 3$ biological replicates. **d** Thr$^{973}$ phosphorylation of AS160 by NEK6 in response to PA. Flag-AS160 WT or mutants were co-expressed with GFP-NEK6 in HEK293 cells. Thr$^{973}$ phosphorylation of AS160 was detected using the site-specific phospho-antibody. **e**, **f** Thr$^{973}$ phosphorylation of endogenous AS160 in NRVCs in response to PA. **e** Representative blots. **f** Quantification data. $n = 7$ biological replicates. **g**, **h** Thr$^{973}$ phosphorylation of endogenous AS160 in the heart of HFD-fed mice administered with or without ZINC05007751 for 8 weeks. **g** Quantification data. **h** Immunoblots. $n = 4$. The data are given as the mean ± SEM. Numbers on the graphs represent $p$ values. Statistical analyses were carried out using two-sided $t$-test for (**c**) and (**f**), and one-way ANOVA for (**g**). Source data are provided as a Source Data file.

on Flag-AS160 (Fig. 6d). PA treatment also increased Thr$^{973}$ phosphorylation on endogenous AS160 in NRVCs (Fig. 6e, f). Moreover, HFD augmented Thr$^{973}$ phosphorylation on endogenous AS160 in mouse heart, and ZINC05007751, a NEK6 inhibitor[32], inhibited HFD-induced AS160-Thr$^{973}$ phosphorylation (Fig. 6g, h). In vitro phosphorylation of MBP-AS160$^{S763\text{-}P1290}$ by Flag-NEK6 inhibited its GAP activity. The inhibition was attenuated by the AS160$^{T973A}$ and AS160$^{T976A}$ single mutations and prevented by the AS160$^{T973/976A}$ double mutation (Fig. 7a). In contrast to NEK6, a related kinase NEK7 did not phosphorylate AS160-Thr$^{973}$ when co-expressed in HEK293 cells (Supplementary Fig. 10f). Moreover, NEK9, an upstream kinase for activating NEK6 and NEK7[33,34], caused no apparent AS160-Thr$^{973}$ phosphorylation when the two proteins were co-expressed in HEK293 cells (Supplementary Fig. 10f). The GAP activities of Flag-tagged mutant AS160$^{T973A}$ and AS160$^{T976A}$ proteins were significantly increased when expressed in WT or AS160-KO HEK293 cells as compared to that of WT Flag-AS160 protein (Fig. 7b, Supplementary Fig. 10g, h). Notably, the single AS160$^{T973A}$ and AS160$^{T976A}$ mutations inhibited, and the AS160$^{T973/976A}$ double mutation prevented, the PA-induced inactivation of AS160 (Fig. 7b, c, Supplementary Fig. 10h). In contrast, mutation of Thr$^{973}$ or Thr$^{976}$ to a phospho-mimic Asp decreased the GAP activity of AS160 to a level similar to PA treatment (Fig. 7d). Moreover, overexpression of GFP-NEK6 caused an inhibition of the GAP activity of Flag-AS160 when the two proteins were co-expressed in HEK293 cells, to an extent comparable to PA treatment (Fig. 7e). NEK6-induced inhibition of AS160 GAP activity was abrogated by AS160$^{T973A}$ or AS160$^{T976A}$ mutation (Fig. 7f). In contrast, knockdown of NEK6 enhanced the GAP activity of endogenous AS160 at the basal state and attenuated PA-induced inhibition of AS160 GAP activity (Fig. 7g, Supplementary Fig. 10i). In agreement, treatment with the NEK6 inhibitor ZINC05007751 also

https://doi.org/10.1038/s41467-024-54031-5

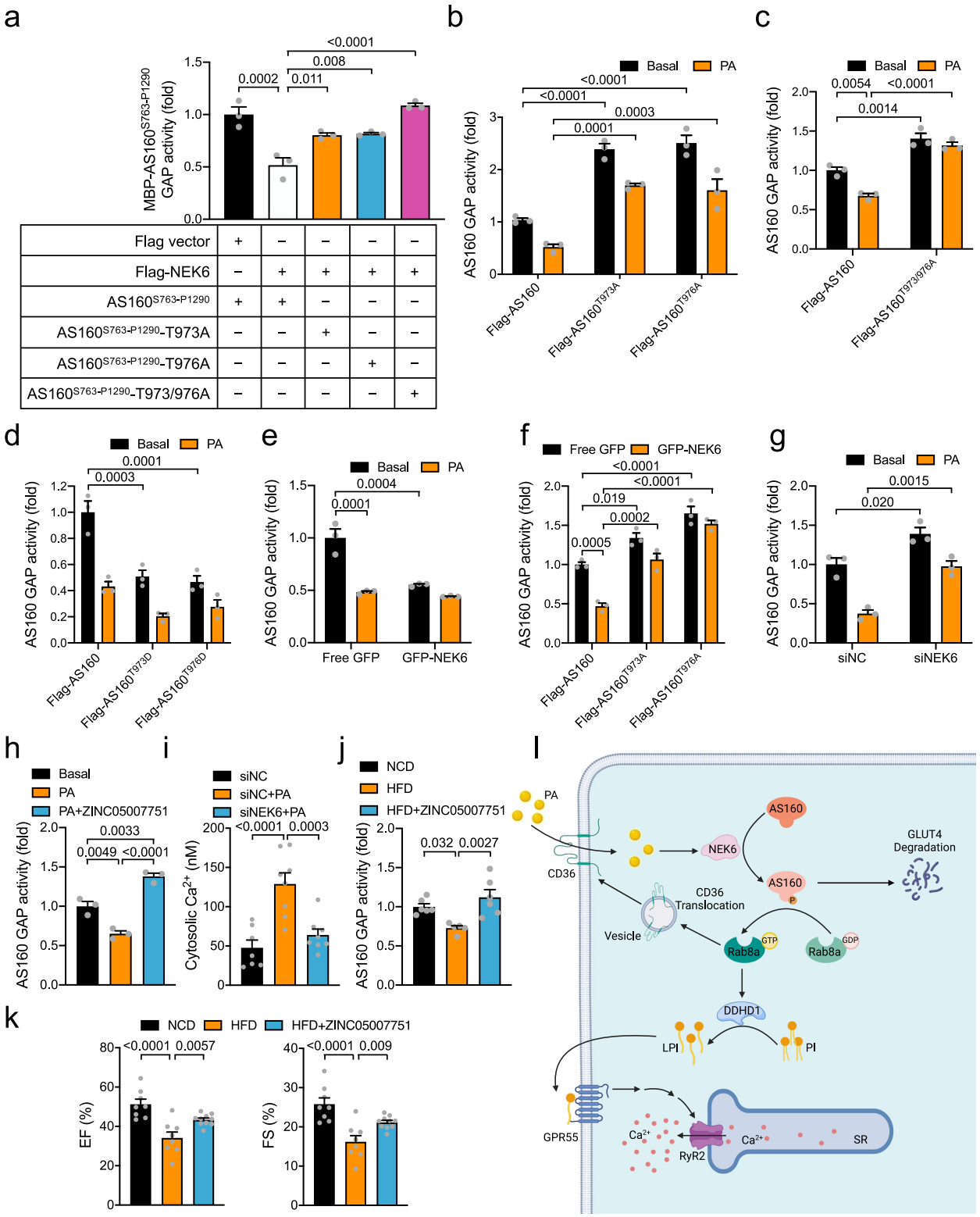


prevented the decrease of AS160 GAP activity in response to PA treatment (Fig. 7h). Importantly, knockdown of NEK6 prevented PA-induced elevation of cytosolic $Ca^{2+}$ in cardiomyocytes (Fig. 7i).

The mRNA and protein levels of NEK6 did not change in the heart of HFD-fed mice (Supplementary Fig. 10j, k). Given the role of NEK6 in mediating PA-induced inactivation of AS160, we wondered whether inhibition of NEK6 might be of therapeutic potential to combat obesity cardiomyopathy. To this end, the NEK6 inhibitor was administered to HFD-fed mice through oral gavage on a daily basis. ZINC05007751 administration did not affect the HFD-induced body weight gain and elevation of blood glucose in mice (Supplementary Fig. 10l, m). At the molecular level, ZINC05007751 did not affect the expression of AS160 in the heart (Supplementary Fig. 10n), but indeed prevented HFD-induced inactivation of AS160 (Fig. 7j). Importantly, the ZINC05007751-treated group on HFD exhibited better cardiac function than the vehicle control group on HFD, as evidenced by higher EF and FS at 6 weeks after ZINC05007751 administration (Fig. 7k). Together, inhibition of NEK6

**Fig. 7 | Regulation of AS160 GAP activity and cardiac function by NEK6. a** GAP activity of recombinant MBP-AS160$^{S763\text{-}P1290}$ WT and mutant proteins upon in vitro phosphorylation by NEK6. $n = 3$ biological replicates. **b** GAP activity of Flag-AS160 WT and mutant proteins in response to PA. HEK293 cells expressing Flag-AS160, Flag-AS160$^{T973A}$ or Flag-AS160$^{T976A}$ were treated with or without PA. $n = 3$ biological replicates. **c** GAP activity of Flag-AS160 WT and mutant proteins in response to PA. HEK293 cells expressing Flag-AS160 or Flag-AS160$^{T973A/T976A}$ were treated with or without PA. $n = 3$ biological replicates. **d** GAP activity of Flag-AS160 WT and mutant proteins in response to PA. AS160-KO HEK293 cells expressing Flag-AS160, Flag-AS160$^{T973D}$ or Flag-AS160$^{T976D}$ were treated with or without PA. $n = 3$ biological replicates. **e** Effects of NEK6 on GAP activity of Flag-AS160 in response to PA. HEK293 cells co-expressing Flag-AS160 with GFP-NEK6 or GFP were treated with or without PA. $n = 3$ biological replicates. **f** Effects of NEK6 on GAP activity of Flag-AS160 WT and mutant proteins. Flag-AS160 WT or mutants was co-expressed with GFP-NEK6 or GFP in HEK293 cells. $n = 3$ biological replicates. **g** GAP activity of endogenous AS160 upon NEK6 knockdown in HEK293 cells in response to PA treatment. $n = 3$ biological replicates. **h** GAP activity of Flag-AS160 in HEK293 cells in response to PA treatment in the presence or absence of NEK6 inhibitor ZINC05007751. $n = 3$ biological replicates. **i** Cytosolic $Ca^{2+}$ in NEK6-knockdown NRVCs in response to PA. $n = 7$ (NC) and 8 (NC + PA, siNEK6+PA) biological replicates. **j** GAP activity of endogenous AS160 in the heart of HFD-fed mice administered with or without ZINC05007751 for 8 weeks. $n = 5$ (NC + PA) and 6 (NC, siNEK6+PA). **k** Cardiac function of HFD-fed mice administered with or without ZINC05007751. EF and FS were measured in HFD-fed mice administered with or without ZINC05007751 for 6 weeks. $n = 8$ (NCD, HFD) and 10 (HFD + ZINC05007751). **l** A diagram (Created in BioRender. Shu S (2022) BioRender.com/y90d330) illustrates the proposed model in which AS160 is a lipid-responsive regulator governing metabolic flexibility and $Ca^{2+}$ homeostasis in the heart. PA/HFD inhibits AS160-GAP activity through phosphorylation by NEK6 in the heart. Inactivation of AS160 causes metabolic remodeling, enhances LPI production and signaling, and impairs $Ca^{2+}$ homeostasis in cardiomyocytes, which may consequently contribute to the development of obesity cardiomyopathy. The data are given as the mean ± SEM. Numbers on the graphs represent $p$ values. Statistical analyses were carried out using one-way ANOVA for (**a**), (**h**–**k**), and two-way ANOVA for (**b**–**g**). Source data are provided as a Source Data file.

by ZINC05007751 exerted a beneficial effect on obesity cardiomyopathy in mice.

## Discussion

In this study, we demonstrate that AS160 functions as a lipid-responsive regulator for cardiac LPI metabolism, $Ca^{2+}$ homeostasis and heart function. Our data are consistent with a model in which cardiac AS160 controls LPI metabolism and consequently regulates $Ca^{2+}$ homeostasis in the heart. AS160 GAP activity is inhibited by PA/HFD in the cardiomyocytes through NEK6-mediated phosphorylation (Fig. 7l). Deletion or inactivation of AS160 in the heart increases LPI metabolism and signaling, impairs $Ca^{2+}$ homeostasis, and eventually causes cardiac dysfunction.

The heart is a well-known insulin-responsive organ that absorbs glucose through GLUT4 upon insulin stimulation. Cardiomyocyte-specific deletion of GLUT4 abolishes insulin-stimulated glucose uptake in the heart and causes modest cardiac hypertrophy with preserved contractile function[23]. Cardiomyocyte-specific GLUT4 deletion elicits a compensatory response to increase GLUT1 expression and consequent basal glucose uptake[23]. The loss of AS160 GAP activity also blunts insulin-stimulated glucose uptake in cardiomyocytes but does not induce upregulation of GLUT1. Instead, deficiency of AS160 decreases GLUT1 expression in the heart at both mRNA and protein levels. Moreover, the AS160-deficient heart develops dilated cardiomyopathy with impaired cardiac contractility. Thus, the loss of AS160 GAP activity in the heart might trigger different responses and result in different pathological consequences as compared to GLUT4 deficiency. As a RabGAP, AS160 may regulate trafficking of other cargoes such as CD36 in cardiomyocytes through its downstream target Rab8a[11], and its deficiency promotes FA utilization in the heart. PA/HFD inhibits the GAP activity of AS160, and decreased AS160-GAP activity promotes CD36 translocation for uptake of FAs into cardiomyocytes, thus forming a feed-forward loop to facilitate FA utilization in obese heart. In addition to CD36 that is a dominant FA transporter in the heart[35], other FA transporters such as FATP4 might also exhibit enhanced surface translocation when AS160 is inactivated and contribute to increased FA utilization in the heart. In skeletal muscle, AS160 deficiency increases total protein expression of FATP4 and thereby augments FA utilization[26]. In contrast, cardiac deletion of AS160 does not elicit such an effect on total FATP4 protein expression. Nevertheless, AS160 deficiency enhances FA utilization in both skeletal muscle and heart although the underlying mechanisms might differ. Our data show that AS160 may be a critical signaling node regulating metabolic flexibility, and its inactivation results in metabolic remodeling to preserve energy production in the heart. More importantly, AS160 also regulates LPI metabolism and signaling in the heart through its downstream target Rab8a, which further impacts on $Ca^{2+}$ homeostasis. Cardiac AS160 deficiency increases LPI levels and consequently impairs $Ca^{2+}$ homeostasis in cardiomyocytes, which may lead to cardiac dysfunction. Therefore, cardiomyopathy resulting from deficiency of AS160, whose GAP activity is inhibited in obesity, resembles obese cardiomyopathy in many aspects including decreased glucose metabolism, increased lipid metabolism, impaired $Ca^{2+}$ homeostasis and reduced cardiac contractility.

LPI is an important signaling metabolite and has been linked to the pathogenesis of metabolic and cardiovascular diseases[36,37]. This phospholipid induces hepatic inflammatory and fibrotic transcriptional changes that promote the pathogenesis of non-alcoholic fatty liver disease[36]. The activation of its receptor GPR55 by LPI triggers myocardial ischemia/reperfusion injury through the Rho kinase/ROCK/p38 MAPK pathway[37]. LPI may directly regulate cardiac contractility through activating GPR55 to mobilize $Ca^{2+}$ from the SR into the cytosol and to elicit depolarization of plasma membrane[29]. The enzymes catalyzing synthesis and degradation of LPI have been recently identified, and their regulation has become a research focus. For example, the phospholipase A2 cPLA2 is a key enzyme converting PI to 1-acyl LPI by the removal of the *sn*−2 fatty acids, whose activity is under the control of phosphorylation by the MAPK[38]. The phospholipase A1 DDHD1 catalyzing the hydrolysis of the *sn*−1 fatty acids of PI to produce 2-acyl LPI is also regulated by protein phosphorylation[39]. Our data demonstrate that AS160 is a key regulator of these two enzymes most likely via its downstream target Rab8a. AS160 and Rab8a both interact with DDHD1 and cPLA2 in cells. Moreover, Rab8a can directly activate DDHD1 in vitro in a manner preferentially dependent on its GTP-bound form. The genetic inactivation of AS160 increases the GTP-bound active Rab8a and thus elevates LPI in the heart, which impairs $Ca^{2+}$ homeostasis and cardiac contractility. Notably, the GAP activity of AS160 is inhibited and Rab8a is consequently activated in the obese heart where $Ca^{2+}$ homeostasis and cardiac contractility are impaired. Therefore, these findings reveal a previously unrecognized regulatory circuit linking AS160 to LPI signaling to regulate $Ca^{2+}$ homeostasis in the heart in response to the HFD.

Insulin is a well-known stimulus regulating AS160 through its phosphorylation by PKB, which inactivates the GAP activity of AS160[10]. Therefore, a general assumption is that the HFD might increase the GAP activity of AS160 through its hypophosphorylation due to the HFD-elicited insulin resistance, which consequently inactivates the Rabs downstream of AS160[40]. In fact, palmitic acid/HFD inactivates the GAP activity of AS160 without affecting the phosphorylation of its Thr$^{642}$, a critical site regulated by insulin[16]. The inactivation of AS160 by palmitic acid/HFD is accompanied by an increase of the GTP-bound active Rab8a. Moreover, insulin causes no further inactivation of

AS160 and activation of Rab8a in the heart of DIO mice. There is a persistent activation of Rab8a in the heart of DIO mice irrespective of insulin stimulation. The HFD-elicited inhibition of AS160 GAP activity in the obese heart is comparable to that elicited by insulin in the heart of mice fed the chow diet. However, the level of active Rab8a in the obese heart is lower than that in the heart of mice fed the chow diet under insulin-stimulated conditions. The GTP-bound state of Rab8a is controlled not only by the GAPs but also by its upstream guanine-nucleotide exchange factors (GEFs) such as Rabin8, GRAB, and MSS4[41,42]. It is possible that insulin, but probably not the HFD, might regulate such a GEF for Rab8a to be fully activated. Nevertheless, the persistent activation of Rab8a due to inactivation of AS160 exerts a profound effect on remodeling lipid metabolism in the heart.

The regulatory mechanism underlying the inactivation of AS160 by PA/HFD is intriguing, and most likely involves $Thr^{973/976}$ phosphorylation of AS160 by NEK6. As a mitotic kinase, NEK6 regulates chromosome congression for mitotic progression via phosphorylating HSP72 and EML4[43,44]. Here, we show that NEK6 is also a regulator of $Ca^{2+}$ homeostasis in cardiomyocytes through phosphorylating AS160. NEK6 expression does not change in the heart of HFD-fed mice at either mRNA or protein levels. Presumably, PA/HFD might upregulate its kinase activity in cardiomyocytes through some mechanism yet to be defined. It has been well established that NEK9 activates NEK6 through phosphorylating $Ser^{206}$ on the NEK6 activation loop[34]. NEK9 itself is activated via phosphorylation by CDK1 and PLK1 during mitosis[45]. It would be intriguing to find out whether NEK6 is activated through a similar regulatory mechanism involving NEK9 or via some other activators in response to PA/HFD. We also note that NEK7, a kinase closely related to NEK6, and NEK9 are also predicted as potential upstream kinases of AS160 using the Scansite (https://scansite4.mit.edu) with medium stringency and might phosphorylate some other sites, but not $Thr^{973}$, on AS160. The potential regulation of AS160 by NEK7 and NEK9 deserves further detailed studies in the future.

In conclusion, AS160 is a regulator for cardiac $Ca^{2+}$ homeostasis through controlling LPI metabolism and signaling. Its GAP activity is inhibited by PA/HFD through NEK6-mediated phosphorylation in the cardiomyocytes. Inhibition of NEK6-mediated phosphorylation of AS160 might be of therapeutic potential to combat obesity cardiomyopathy.

## Methods

This study was carried out under approval of the Ethics Committee of Nanjing University complying with all relevant ethical regulations. All animal procedures involving mice and rats in this study were approved by the Institutional Animal Care and Use Committee (IACUC) at Model Animal Research Center of Nanjing University. The experimental protocol involving monkeys was approved by the Institutional Animal Care and Use Committee of Peking University.

### Materials

Recombinant human insulin was bought from Novo Nordisk (Bagsvaerd, Denmark). 2-deoxy-D-[1,2-$^3$H(N)]glucose was purchased from PerkinElmer (American Fork, UT, USA). Protein G-Sepharose was bought from GE Healthcare (Little Chalfont, Buckinghamshire, UK). ZINC05007751 (E2511) was bought from Selleck (Shanghai, China) and CID16020046 (HY16697) was from MedChemExpress (Shanghai, China). All other chemicals were from Sigma-Aldrich (Shanghai, China) or Sangon Biotech (Shanghai, China). The commercial primary antibodies are listed in Supplementary Table 1, and used for immunoblotting at a dilution of 1:1000. Horseradish peroxidase (HRP)-conjugated mouse anti-rabbit IgG (211-002-171), goat anti-rabbit IgG (Cat No. 111-035-003), goat anti-mouse IgG (Cat No. 115-035-003), and light chain specific goat anti-mouse IgG (115-005-174) were bought from Jackson ImmunoResearch Laboratories, and used at 1:5000 dilution. Site-specific $pThr^{973}$-AS160 antibody was raised in rabbit using the synthetic phosphopeptide CHAILVDLGR(p)TFPTHPY (Cys for coupling, plus residues 964 to 979 of mouse AS160, where pT represents phosphorylated $Thr^{973}$) at Affinity Biosciences (Changzhou, China).

### Molecular biology

The cDNAs encoding human AS160 (NP_055647.2), mouse cPLA2 (NP_032895.1), mouse DDHD1 (NP_001036184.1), mouse Rab8a (NP_075615.2), human NEK6 (NP_001138473.1), mouse PLD3 (NP_001304284.1), mouse ABHD6 (NP_079617.2), mouse AGPAT8 (NP_001074540.1), mouse MBOAT7 (NP_084210.2), mouse NEK7 (NP_067618.1), and mouse NEK9 (NP_660120.2) were cloned into pcDNA5-FRT/TO vectors with tags for expression in mammalian cells. All plasmids were sequenced at AZENTA Life Science (Suzhou, China).

### Cell culture, transfection and stimulation

Human embryonic kidney HEK293 cells (Cat No. 1101HUM-PUMC000091) and rat H9C2 cardiomyocytes (Cat No. 1101RAT-PUMC000219) obtained from the Cell Resource Center, Chinese Academy of Medical Sciences and Peking Union Medical College (China) were cultured in DMEM medium containing 10% (v/v) foetal bovine serum and monitored with regular mycoplasma tests. Transfections of plasmids were carried out in HEK293 cells using a PEI-mediated method.

Human induced pluripotent stem cell-derived cardiomyocytes (hiPSC-CMs) were obtained from the Beijing Laboratory for Cardiovascular Precision Medicine (Capital Medical University, China), and cultured in CardioEasy human cardiomyocyte maintenance medium (Cellapy, CA2015002).

HEK293 cells and H9C2 cardiomyocytes were incubated with or without BSA-conjugated PA or OA (200 μM, 30 min) for acute treatments. For chronic treatment, cardiomyocytes were incubated with 50 μM PA for 12 h.

### Rodent breeding, husbandry, and treatments

The Ethics Committee at Model Animal Research Center of Nanjing University reviewed and approved all mouse and rat procedures used in this study. Mice (C57Bl6J background) and rats (Sprague Dawley) were raised on normal chow diet (14.9 kcal% fat, #1010013, Jiangsu Xietong Pharmaceutical Bio-engineering Co., Ltd, China) in an animal house free of specific pathogens with a light/dark cycle of 12 h.

The global AS160 knockout (exon 6 and 7 deleted), $AS160^{f/f}$ and $AS160^{R972K}$ mice (numbering according to NP_001391600.1, previously known as $AS160^{R917K}$ according to NP_001074747.2) were generated previously[14]. The αMHC-Cre[21] mice with a C57Bl/6J background were purchased from the Nanjing Biomedical Research Institute of Nanjing University, and mated with the $AS160^{f/f}$ mice to generate cardiomyocyte-specific AS160 knockout mice. Global AS160 knockout and $AS160^{R972K}$ knockin homozygotes and their corresponding WT littermate controls were produced from heterozygote X heterozygote mating and used in experiments. As for cardiomyocyte-specific knockout mice, the $AS160^{f/f}$ mice were mated with the $AS160^{f/f}$/αMHC-Cre mice to generate $AS160^{f/f}$ (control mice) and $AS160^{f/f}$/αMHC-Cre (cardiomyocyte-specific AS160 knockout mice, AS160-cKO). Genotyping was performed as previously described[14].

The NEK6 inhibitor, ZINC05007751 (100 mg/kg/day), was administered via oral gavage once a day to mice fed HFD (60 kcal% fat, D12492, Research Diets, USA). In vivo, FA treatment was carried out as previously described[46]. Briefly, mice were deprived of food for 4 h, and orally administered with PA (500 mg/10 ml 10% olive oil /kg body weight), OA (500 mg/10 ml 10% olive oil /kg body weight) or a vehicle control (10% olive oil, 10 ml/kg body weight). Mice were sacrificed 3 h after the oral administration of PA/OA for tissue harvest.

### Monkey housing

The monkeys (rhesus macaques) used in this study were housed individually in cages, under a 12-h light–dark cycle at 18–24 °C and 40–70% humidity. The monkeys had free access to water and were fed *ad libitum* with national standard pellet monkey chow (Beijing HFK Bio-Technology Co., Ltd, China), which contains 7–10% crude fat, 16–20% crude protein, and 55–65% crude carbohydrate. The experimental protocol was approved by the Institutional Animal Care and Use Committee of Peking University (IMM-ZhangXQ-1) and followed the principles of laboratory animal care of the China National Academy of Sciences/National Research Council. The heart tissues were harvested from monkeys euthanized because of incurable diseases such as abdominal aortic embolism, myocardial infarction, heart failure, or severe diabetes etc.

### Blood chemistry

Blood glucose levels were determined using a Breeze-2 glucometer (Bayer). Serum triglyceride (TG), non-esterified fatty acid (NEFA), and total cholesterol (TC) were measured with the Wako LabAssay Triglyceride (290-63701), LabAssay NEFA kit (294-63601) and LabAssay Cholesterol kit (294-65801) (Wako Chemicals USA), respectively.

### Echocardiography (Echo)

Mice were anaesthetized with gaseous isoflurane and subjected to Echo assay using a Vevo 770 high-resolution in vivo micro-imaging system (VisualSonics, inc) with a 30 MHz RMV-707B ultrasonic probe as previously described[17]. The ultrasonic probe was positioned with a 90° angle between the probe and the heart for collection of M-mode pictures. Left ventricle anterior wall (LVAW), left ventricle posterior wall (LVPW), left ventricle internal dimension (LVID), and left ventricle volume (LV Vol) of systole and diastole were measured on the M-mode images and averaged from 6 cardiac cycles. The formulas for calculation of ejection fraction (EF) and fraction shortening (FS) are as follows, EF% = [(LV Vol;d - LV Vol;s)/LV Vol;d] × 100%, and FS % = [(LVID;d−LVID;s)/LVID;d] × 100%. Diastolic function was measured using the Vevo3100 system (VisualSonics, inc). The early peak velocity (E) and late peak velocity (A) of mitral valve were determined, and the E/A ratio was calculated as a measure of diastolic function.

### Generation of AS160-KO HEK293 cells

Human embryonic kidney HEK293 cells were obtained from the Cell Resource Center, Chinese Academy of Medical Sciences and Peking Union Medical College (China), and maintained in DMEM medium containing 10% (v/v) foetal bovine serum. HEK293 cells were transfected with plasmids using Lipofectamine 3000 reagent (Thermo Fisher Scientific). AS160-KO HEK293 cells were generated using the CRISPR/Cas9 system. The sgRNA sequences targeting AS160 were 5′-TGTTTCAGGACTACTCACCA-3′ and 5′-ACTCCCCGCAGTTTCGAAGA-3′.

### Glucose uptake assay in neonatal mouse cardiomyocytes

Primary mouse cardiomyocytes were isolated from neonatal mice (1-day-old) using a collagenase-based method and cultured as previously described[47]. Briefly, neonatal hearts were minced finely with scissors and digested with a collagenase solution (1 mg/ml). Isolated primary cardiomyocytes were cultured in DMEM (65%)/M199 (19%) medium plus foetal bovine serum (5%)/horse serum (10%) and penicillin/streptomycin (1%) for 18–24 h. After settling down, primary cardiomyocytes were further cultured in DMEM (78%)/M199 (17%) plus horse serum (4%) and penicillin/streptomycin (1%).

Glucose uptake was carried out in primary cardiomyocytes from neonatal mice as previously described[48]. Briefly, primary cardiomyocytes were stimulated with or without 100 nM insulin for 30 min, and then incubated in uptake buffer containing 2-deoxy-D-[1,2-$^3$H(N)] glucose for a further 10 min in the presence or absence of insulin. The uptake assay was then terminated, and radioisotopes in cell lysates were determined using a Tri-Carb 2800TR scintillation counter (PerkinElmer). Protein concentrations in cell lysates were determined and used for normalization of glucose uptake rates.

### In vivo glucose uptake assay

In vivo, glucose uptake into the heart was performed using a fluorescent d-glucose analog 2-[N-(7-nitrobenz-2-oxa-1,3-diazol-4-yl) amino]−2-deoxy-D-glucose (2-NBDG). Briefly, mice were fasted overnight and refed for 1 h on the following day. Afterwards, mice were intravenously administered with 2-NBDG (200 μM in 100 μl PBS) and injected intraperitoneally with heparin sodium. Mice injected intravenously with 100 μl PBS were used as controls. Hearts were harvested at 15 min after administration of 2-NBDG. After being perfused with PBS, hearts were weighed and homogenized in 2 ml lysis buffer. Homogenates were centrifugated at 18,000 rpm for 5 min, and resultant supernatants were used to measure fluorescent signals of 2-NBDG at 475 nm excitation and 550 nm emission using a microplate reader (Synergy H1, BioTek Instruments Inc). The fluorescent signals were normalized to heart weights.

### Fatty acid uptake in cardiomyocytes

Primary cardiomyocytes were isolated from adult mouse heart that was perfused with 1 mg/ml collagenase through a Langendorff system (ADInstruments). Tissue debris was removed using a cell strainer (100 μm of mesh size) after collagenase digestion, and resultant cardiomyocytes were resuspended in Hanks buffer. After being stimulated with or without insulin in Hank's buffer for 30 min, primary cardiomyocytes were incubated with BODIPY 558/568-C12 (D-3835, Thermo Fisher Scientific) for 10 min. BODIPY 558/568-C12 inside cells were measured using a microplate reader (Synergy H1, BioTek Instruments Inc) after cell lysis and used to calculate fatty acid uptake rates.

TAMRA-PA and TAMRA-OA were obtained from Ruixi Biological Technology Co. Ltd (Xi'an, China), and used for uptake assay in H9C2 cardiomyocytes. The fluorophore-conjugated PA or OA (10 μM) was added to H9C2 cardiomyocytes, and images were taken at the indicated time intervals using a Leica SP5 confocal microscope.

### In vivo fatty acid uptake assay

In vivo, fatty acid uptake into the heart was performed using fluorescent BODIPY-FL-C16 (Thermofisher, D3821) as previously described with modifications[49]. Briefly, mice were fasted overnight and refed for 1 h on the following day. Afterwards, mice were intravenously administered with BODIPY-FL-C16 (200 μM bound to 1% BSA in 100 μl PBS) and injected intraperitoneally with heparin sodium. Mice injected intravenously with 100 μl PBS were used as controls. After 20 min, hearts were harvested, perfused, weighed, and homogenized in 2 ml lysis buffer. Homogenates were centrifugated at 17,000 × *g* for 5 min, and resultant supernatants were used to measure fluorescent signals of BODIPY-FL-C16 at 488 nm excitation and 515 nm emission using the microplate reader (Synergy H1, BioTek Instruments Inc). The fluorescent signals were normalized to heart weights.

### Measurement of cell surface GLUT4, CD36 and FATP4

A biotinylation-based method was used to measure cell surface GLUT4, CD36 and FATP4. Primary cardiomyocytes were stimulated with or without insulin for 30 min and then incubated with Sulfo-NHS-SS-Biotin (Thermo Fisher Scientific) in Hanks buffer (+/- insulin) for 30 min. Afterwards, cardiomyocytes were lysed, and biotinylated surface GLUT4, CD36, and FATP4 were isolated using NeutrAvidin-Agarose (Thermo Fisher Scientific) and determined via immunoblotting using the respective antibodies.

### Gene knockdown in primary neonatal rat cardiomyocytes

Primary neonatal rat cardiomyocytes were isolated from ventricles of neonatal Sprague Dawley rats (postnatal day 0–3) via sequential digestion with trypsin (0.25%) at 4 °C overnight and collagenase (1 mg/ml) at 37 °C for 15 min. Neonatal rat cardiomyocytes were cultured in DMEM supplemented with 10% (v/v) foetal bovine serum, and transfected with siRNAs using Lipofectamine 3000 reagent (Thermo Fisher Scientific). The siRNA sequences targeting rat genes are as follows. siAS160: 5′-GAGCCAAGCUGGUAAUCCATT-3′. siRab8a: 5′-GGAAUAAGUGUGAUGUGAATT-3′. siNEK6: 5′-AGACAGUGGCUCUGAAGAATT-3′.

### $Ca^{2+}$ imaging in primary cardiomyocytes

$Ca^{2+}$ transients were measured in primary cardiomyocytes using a Fluo-4-AM based method[50]. Briefly, cardiomyocytes were loaded with Fluo-4-AM in Hanks buffer containing 1 mM $MgCl_2$, 1 mM $CaCl_2$, 5.56 mM glucose, 2 mM pyruvate, and 2% (w/v) BSA (VWR, Cat No. 0332), and subsequently stimulated with a GRASS S48 stimulator (frequency 0.5 Hz, duration 60 ms, decay 40 ms, voltage 80 V, repeat). $Ca^{2+}$ transients were determined on line-scan images of cardiomyocytes taken with a Zeiss LSM880 confocal microscope using IDL5.5 (Harris Geospatial Solutions). The decay time (Tau) of $Ca^{2+}$ transients was referred to the time elapsing from the peak of $Ca^{2+}$ transients to 63% from the peak to the basal level in the fading phase.

$Ca^{2+}$ sparks were measured in $Ca^{2+}$-loaded primary cardiomyocytes that were incubated with 5 μM Fluo-4-AM (Thermo Fisher Scientific). Images of cardiomyocytes were taken using a Zeiss LSM880 confocal microscope.

### Measurement of cytosolic $Ca^{2+}$

Intracellular $Ca^{2+}$ concentration was determined using the $Ca^{2+}$ indicator Fura-2/AM as previously described[51]. H9C2 or neonatal rat cardiomyocytes were washed with HBSS buffer (pH = 7.2) supplemented with 1 mM $CaCl_2$ and 1 mM $MgCl_2$ and then stained with 5 μM Fura-2/AM at 37 °C for 25 min. After three times of washes with HBSS buffer, fluorescent signals in cells were detected using a microplate reader (Synergy H1, BioTek Instruments Inc) with excitation at 340 nm and 380 nm, respectively. Cytosolic $Ca^{2+}$ was calculated using the following equation, $[Ca^{2+}]_i = Kd \times (F_D/F_S) \times [(R\text{-}R_{min})/(R_{max}\text{-}R)]$, in which R is the average ratio of fluorescence (340/380) for a preset time, $R_{min}$ is the ratio of fluorescence (340/380) of cells treated with 25 mM EGTA, and $R_{max}$ is the ratio of fluorescence (340/380) of cells treated with 0.1% Triton X-100 in the presence of 10 mM $CaCl_2$ and 10 mM $MgCl_2$. $F_D$ is the fluorescence at 380 nm of cells treated with 25 mM EGTA, and $F_S$ is the fluorescence at 380 nm of cells treated with 0.1% Triton X-100 in the presence of 10 mM $CaCl_2$ and 10 mM $MgCl_2$. Kd is the dissociation constant between $Ca^{2+}$ and Fura-2/AM, which is 224 nmol/l.

### SR $Ca^{2+}$ load in primary cardiomyocytes

SR $Ca^{2+}$ load was measured in primary cardiomyocytes as previously described[52]. Briefly, twitch characteristics of cardiomyocytes were stabilized through pacing with electrical stimulation at 0.5 Hz. When fully paced, cardiomyocytes were stimulated with caffeine (10 mM) to elicit $Ca^{2+}$ release from the SR. Line-scan images were taken using a Zeiss LSM880 confocal microscope and analyzed with IDL5.5. The amplitude of $Ca^{2+}$ transient induced by caffeine was determined and used as an index of SR $Ca^{2+}$ load.

### Measurement of cardiomyocyte contractility

Primary cardiomyocytes were loaded with 2 μM Fura-2/AM and treated with or without 45 μM CID16020046 simultaneously. Cardiomyocyte contractility and $Ca^{2+}$ transients were induced by electrical pacing at 0.5 Hz as previously described[53]. Cardiomyocyte contractility and $Ca^{2+}$ handling were measured using the Myocyte Calcium and Contractility System (IonOptix LLC FSI800).

### Measurement of L-type $Ca^{2+}$ current

The L-type $Ca^{2+}$ current of mouse primary cardiomyocytes was measured in a $Na^+$- and $K^+$-free solution as described previously[54]. Briefly, the chamber was initially perfused with solution containing 142 mM NaCl, 5.4 mM KCl, 1.8 mM $CaCl_2$, 0.5 mM $MgCl_2$, 0.33 mM $NaH_2PO_4$, 5.5 mM glucose, 5 mM HEPES (pH adjusted to 7.4 with NaOH). After obtainment of a gigaohm seal, the external solution was changed to a $Na^+$- and $K^+$-free buffer (140 mM TEA-Cl, 5 mM $CaCl_2$, 2 mM $MgCl_2$, 10 mM glucose, 10 mM HEPES (pH adjusted to 7.4 with TEA-OH)) and 10 μM tetrodotoxin. The solution of patch pipettes contains 120 mM CsCl, 10 mM TEA-Cl, 5 mM $Cs_4$-BAPTA, 5 mM MgATP, 10 mM HEPES (pH adjusted to 7.3 with CsOH). Patch electrode resistances were 0.5–2.5 MΩ. The current / voltage curves of LTCC were recorded with −80 to +70 mV steps (10 mV interval and 200 ms for each step), at −40 holding potential. The LTCC inactivation was recorded with potential transition to +20 mV from −40 to +10 mV steps (5 mV interval). The window currents were measured in −40 to +10 mV steps (5 mV interval and 1.5 s for each step) following 20 mV holding. All electrophysiological data were detected using a MultiClamp 700B amplifier and Digidata 1550 data acquisition system (Axon Instruments). Current was sampled at 10 kHz and filtrated under 2 kHz.

### Measurement of AS160 GAP activity

The GAP activity of immunoprecipitated endogenous AS160 or Flag-tagged AS160 was measured using recombinant Rab8a as substrate. Phosphate released from hydrolysis of GTP during the reaction was determined using the ascorbic acid-ammonium molybdate reagent as described[55].

### Measurement of GTP-bound form of Rab8a

GTP-bound Rab8a was measured via a pulldown assay as previously described[48]. Briefly, mouse heart or H9C2 cardiomyocytes were lysed in lysis buffer (50 mM HEPES/KOH pH 7.4, 100 mM NaCl, 4 mM $MgCl_2$, 1 mM DTT, 1% NP-40, 10% glycerol, 10 mM NaF, 1 mM $Na_3VO_4$, 1 μg/ml Leupeptin, 1 μg/ml Pepstatin and 1 μg/ml Aprotinin). Purified recombinant GST-Optineurin protein was added to tissue/cell lysates and incubated at 4 °C overnight. Afterwards, glutathione-Sepharose beads were added to capture the GST-Optineurin/GTP-Rab8a complex. Non-specific binding proteins were removed via intensive washing of resins, and GTP-Rab8a bound to GST-Optineurin was eluted in SDS sample buffer and detected via immunoblotting.

### Measurement of DDHD1 activity

Flag-DDHD1 was expressed in HEK293 cells and purified using Flag beads. Purified Flag-DDHD1 was incubated with 20 μM PI (38:4, Avanti, #850144 P) in an assay buffer (100 mM Hepes (pH = 7.5), 80 μM C12E8, 2.5 μM 17:0 LPC, 0.6 μM PIP2) in the presence of MBP, or GDP- or GTPγS-loaded MBP-Rab8a. After extraction with methanol/acetonitrile (80/20, v/v), resultant LPI20:4 was measured using a LC-QTOF mass-spectrometry (Agilent, 6500 QTOF) and used to calculate DDHD1 activity.

### Cardiac lipidomics

The lipidomics study was performed at LipidALL Technologies (Beijing, China) as previously described[56]. Briefly, heart tissue powders were extracted using a Chloroform:methanol-based method. Cardiac lipid extracts were analyzed via an Exion UPLC coupled to a QTRAP 6500 PLUS mass spectrometry (Sciex). Quantification of lipids was performed through adding internal standards of corresponding lipid species and normalized to tissue weight.

### Tissue lysis and measurement of protein concentration

Mouse tissues were rapidly harvested, snap-frozen in liquid nitrogen, and lysed after homogenization using a Polytron homogenizer (Kinematica, Luzern, Switzerland) as previously described[48]. Protein concentrations of tissue homogenates were measured using Bradford reagent (Thermo Fisher Scientific).

### Immunoprecipitation and immunoblotting

Proteins of interest were immunoprecipitated from tissue or cell lysates with antibody-coupled protein G-Sepharose or Flag beads (Sigma).

Lysates or immunoprecipitates were electrophoretically separated via SDS-PAGE and immunoblotted onto nitrocellulose membranes. Afterwards, membranes were subjected to sequential incubation with primary antibodies and horseradish-peroxidase-conjugated secondary antibodies. Non-specific bound antibodies were removed through intensive washing, and membranes were then incubated with ECL substrates (GE Healthcare, UK). Chemiluminescence signals were detected and recorded using a gel documentation system (Syngene, UK). Immunoblotting signals were quantified using ImageJ (version 1.46), and normalized with internal loading controls.

### In vitro phosphorylation

Flag-NEK6 was expressed in HEK293 cells and purified using Flag beads. The purified Flag-NEK6 protein was used to phosphorylate AS160-NEKtide (LVDLGRtFPtHP, $Thr^{973/976}$ shown in lower case) or purified MBP-$AS160^{S763\text{-}P1290}$ recombinant proteins in vitro at 30 °C for 30 min as previously described[57].

### RNA isolation and quantitative PCR (QPCR)

Total RNA was extracted from the heart using the TRIzol® Reagent (Life Technologies), and used to for reverse-transcription into cDNA using a PrimeScript® RT reagent kit (DRR047A, TaKaRa). QPCR was carried out to measure expression levels of target genes using an Applied Biosystems® StepOnePlus™ Real-Time PCR system (Life Technologies). The primers for QPCR were listed in Supplementary Table 2.

### Statistical analysis and reproducibility

Data analyses were performed via two-sided *t*-test or nested *t*-test for two groups, or via one-way ANOVA, two-way ANOVA or nested two-way ANOVA for multiple groups using Prism v9.5.1 software (GraphPad, San Diego, CA, USA). Differences were considered statistically significant at $p < 0.05$.

No statistical method was used to predetermine sample size. Samples were randomly allocated into experimental groups. The Investigators were not blinded to allocation during experiments and outcome assessment. No data were excluded from the analyses. Similar results were obtained from at least two experiments for Figs. 1c, h, 5b–g, j, 6a, d.

### Reporting summary

Further information on research design is available in the Nature Portfolio Reporting Summary linked to this article.

## Data availability

All data generated or analyzed during this study are included in this published article (and its supplementary information files). The source data underlying Figs. 1a-m, 2a-g, 3b-d, f-h, j, 4b-e, g-j, 5b-m, 6a-h, 7a-k, and Supplementary Figs. 1a, c-1, 2a-f, 3a-o, 4a-u, 5a-d, 6a-i, k, m, 7a-e, 8a-e, 9a-g, i-j, and 10b-n are provided as a Source Data file. Source data are provided with this paper.

## References


1. Wong, C. & Marwick, T. H. Obesity cardiomyopathy: pathogenesis and pathophysiology. *Nat. Clin. Pract. Cardiovasc. Med.* **4**, 436–443 (2007).
2. Wong, C. & Marwick, T. H. Obesity cardiomyopathy: diagnosis and therapeutic implications. *Nat. Clin. Pract. Cardiovasc. Med.* **4**, 480–490 (2007).
3. Ren, J., Wu, N. N., Wang, S., Sowers, J. R. & Zhang, Y. Obesity cardiomyopathy: evidence, mechanisms, and therapeutic implications. *Physiol. Rev.* **101**, 1745–1807 (2021).
4. Nakamura, M. & Sadoshima, J. Cardiomyopathy in obesity, insulin resistance and diabetes. *J. Physiol.* **598**, 2977–2993 (2020).
5. Ouwens, D. M. et al. Cardiac contractile dysfunction in insulin-resistant rats fed a high-fat diet is associated with elevated CD36-mediated fatty acid uptake and esterification. *Diabetologia* **50**, 1938–1948 (2007).
6. Ritchie, R. H. & Abel, E. D. Basic mechanisms of diabetic heart disease. *Circ. Res.* **126**, 1501–1525 (2020).
7. Jia, G., DeMarco, V. G. & Sowers, J. R. Insulin resistance and hyperinsulinaemia in diabetic cardiomyopathy. *Nat. Rev. Endocrinol.* **12**, 144–153 (2016).
8. Moltke, I. et al. A common Greenlandic TBC1D4 variant confers muscle insulin resistance and type 2 diabetes. *Nature* **512**, 190–193 (2014).
9. Manousaki, D. et al. Toward precision medicine: TBC1D4 disruption is common among the inuit and leads to underdiagnosis of type 2 diabetes. *Diabetes Care* **39**, 1889–1895 (2016).
10. Sano, H. et al. Insulin-stimulated phosphorylation of a Rab GTPase-activating protein regulates GLUT4 translocation. *J. Biol. Chem.* **278**, 14599–14602 (2003).
11. Samovski, D., Su, X., Xu, Y., Abumrad, N. A. & Stahl, P. D. Insulin and AMPK regulate FA translocase/CD36 plasma membrane recruitment in cardiomyocytes via Rab GAP AS160 and Rab8a Rab GTPase. *J. Lipid Res.* **53**, 709–717 (2012).
12. Sano, H. et al. Rab10, a target of the AS160 Rab GAP, is required for insulin-stimulated translocation of GLUT4 to the adipocyte plasma membrane. *Cell Metab.* **5**, 293–303 (2007).
13. Chen, Q. et al. Rab8a deficiency in skeletal muscle causes hyperlipidemia and hepatosteatosis by impairing muscle lipid uptake and storage. *Diabetes* **66**, 2387–2399 (2017).
14. Xie, B. et al. The Inactivation of RabGAP function of AS160 promotes lysosomal degradation of GLUT4 and causes postprandial hyperglycemia and hyperinsulinemia. *Diabetes* **65**, 3327–3340 (2016).
15. Yang, X. et al. Tissue-specific splicing and dietary interaction of a mutant As160 allele determine muscle metabolic fitness in rodents. *Diabetes* **70**, 1826–1842 (2021).
16. Chen, S., Wasserman, D. H., MacKintosh, C. & Sakamoto, K. Mice with AS160/TBC1D4-Thr649Ala knockin mutation are glucose intolerant with reduced insulin sensitivity and altered GLUT4 trafficking. *Cell Metab.* **13**, 68–79 (2011).
17. Quan, C., Xie, B., Wang, H. Y. & Chen, S. PKB-mediated Thr649 phosphorylation of AS160/TBC1D4 regulates the R-Wave amplitude in the heart. *PLoS ONE* **10**, e0124491 (2015).
18. Binsch, C. et al. Deletion of Tbc1d4/As160 abrogates cardiac glucose uptake and increases myocardial damage after ischemia/reperfusion. *Cardiovasc. Diabetol.* **22**, 17 (2023).
19. Roach, W. G., Chavez, J. A., Miinea, C. P. & Lienhard, G. E. Substrate specificity and effect on GLUT4 translocation of the Rab GTPase-activating protein Tbc1d1. *Biochem. J.* **403**, 353–358 (2007).
20. Wu, K. M. et al. High-density lipoprotein ameliorates palmitic acid-induced lipotoxicity and oxidative dysfunction in H9c2 cardiomyoblast cells via ROS suppression. *Nutr. Metab.* **16**, 36 (2019).
21. Agah, R. et al. Gene recombination in postmitotic cells. Targeted expression of Cre recombinase provokes cardiac-restricted, site-specific rearrangement in adult ventricular muscle in vivo. *J. Clin. Invest.* **100**, 169–179 (1997).
22. Paiman, E. H. M. et al. Phenotyping diabetic cardiomyopathy in Europeans and South Asians. *Cardiovasc. Diabetol.* **18**, 133 (2019).

23. Abel, E. D. et al. Cardiac hypertrophy with preserved contractile function after selective deletion of GLUT4 from the heart. *J. Clin. Invest.* **104**, 1703–1714 (1999).
24. Luiken, J. J. et al. Insulin stimulates long-chain fatty acid utilization by rat cardiac myocytes through cellular redistribution of FAT/CD36. *Diabetes* **51**, 3113–3119 (2002).
25. Habets, D. D. et al. AMPK-mediated increase in myocardial long-chain fatty acid uptake critically depends on sarcolemmal CD36. *Biochem. Biophys. Res. Commun.* **355**, 204–210 (2007).
26. Benninghoff, T. et al. The RabGAPs TBC1D1 and TBC1D4 control uptake of long-chain fatty acids into skeletal muscle via fatty acid transporter SLC27A4/FATP4. *Diabetes* **69**, 2281–2293 (2020).
27. Jain, S. S. et al. Additive effects of insulin and muscle contraction on fatty acid transport and fatty acid transporters, FAT/CD36, FABPpm, FATP1, 4 and 6. *FEBS Lett.* **583**, 2294–2300 (2009).
28. Cheng, H. & Lederer, W. J. Calcium sparks. *Physiol. Rev.* **88**, 1491–1545 (2008).
29. Yu, J. et al. Differential activation of cultured neonatal cardiomyocytes by plasmalemmal versus intracellular G protein-coupled receptor 55. *J. Biol. Chem.* **288**, 22481–22492 (2013).
30. Kargl, J. et al. A selective antagonist reveals a potential role of G protein-coupled receptor 55 in platelet and endothelial cell function. *J. Pharmacol. Exp. Ther.* **346**, 54–66 (2013).
31. Yamashita, A. et al. The actions and metabolism of lysophosphatidylinositol, an endogenous agonist for GPR55. *Prostaglandins Other Lipid Mediat.* **107**, 103–116 (2013).
32. De Donato, M. et al. Identification and antitumor activity of a novel inhibitor of the NIMA-related kinase NEK6. *Sci. Rep.* **8**, 16047 (2018).
33. Haq, T. et al. Mechanistic basis of Nek7 activation through Nek9 binding and induced dimerization. *Nat. Commun.* **6**, 8771 (2015).
34. Belham, C. et al. A mitotic cascade of NIMA family kinases. Nercc1/Nek9 activates the Nek6 and Nek7 kinases. *J. Biol. Chem.* **278**, 34897–34909 (2003).
35. Glatz, J. F., Nabben, M., Heather, L. C., Bonen, A. & Luiken, J. J. Regulation of the subcellular trafficking of CD36, a major determinant of cardiac fatty acid utilization. *Biochim. Biophys. Acta* **1861**, 1461–1471 (2016).
36. Helsley, R. N. et al. Obesity-linked suppression of membrane-bound O-acyltransferase 7 (MBOAT7) drives non-alcoholic fatty liver disease. *eLife* **8** https://doi.org/10.7554/eLife.49882 (2019).
37. Robertson-Gray, O. J. et al. l-alpha-Lysophosphatidylinositol (LPI) aggravates myocardial ischemia/reperfusion injury via a GPR55/ROCK-dependent pathway. *Pharmacol. Res. Perspect.* **7**, e00487 (2019).
38. Leslie, C. C. Cytosolic phospholipase A(2): physiological function and role in disease. *J. Lipid Res.* **56**, 1386–1402 (2015).
39. Matsumoto, N. et al. Phosphorylation of human phospholipase A1 DDHD1 at newly identified phosphosites affects its subcellular localization. *J. Biol. Chem.* **297**, 100851 (2021).
40. Mafakheri, S., Chadt, A. & Al-Hasani, H. Regulation of RabGAPs involved in insulin action. *Biochem. Soc. Trans.* **46**, 683–690 (2018).
41. Guo, Z., Hou, X., Goody, R. S. & Itzen, A. Intermediates in the guanine nucleotide exchange reaction of Rab8 protein catalyzed by guanine nucleotide exchange factors Rabin8 and GRAB. *J. Biol. Chem.* **288**, 32466–32474 (2013).
42. Itzen, A., Pylypenko, O., Goody, R. S., Alexandrov, K. & Rak, A. Nucleotide exchange via local protein unfolding-structure of Rab8 in complex with MSS4. *EMBO J.* **25**, 1445–1455 (2006).
43. O'Regan, L. et al. Hsp72 is targeted to the mitotic spindle by Nek6 to promote K-fiber assembly and mitotic progression. *J. Cell Biol.* **209**, 349–358 (2015).
44. Adib, R. et al. Mitotic phosphorylation by NEK6 and NEK7 reduces the microtubule affinity of EML4 to promote chromosome congression. *Sci. Signal* **12**, eaaw2939 (2019).
45. Bertran, M. T. et al. Nek9 is a Plk1-activated kinase that controls early centrosome separation through Nek6/7 and Eg5. *EMBO J.* **30**, 2634–2647 (2011).
46. Yang, Z. H., Takeo, J. & Katayama, M. Oral administration of omega-7 palmitoleic acid induces satiety and the release of appetite-related hormones in male rats. *Appetite* **65**, 1–7 (2013).
47. Xu, X. et al. ASF/SF2-regulated CaMKIIdelta alternative splicing temporally reprograms excitation-contraction coupling in cardiac muscle. *Cell* **120**, 59–72 (2005).
48. Chen, L. et al. Disruption of the AMPK-TBC1D1 nexus increases lipogenic gene expression and causes obesity in mice via promoting IGF1 secretion. *Proc. Natl Acad. Sci. USA* **113**, 7219–7224 (2016).
49. Nie, B. et al. Specific bile acids inhibit hepatic fatty acid uptake in mice. *Hepatology* **56**, 1300–1310 (2012).
50. Zhu, S. et al. The RalGAPalpha1-RalA signal module protects cardiac function through regulating calcium homeostasis. *Nat. Commun.* **13**, 4278 (2022).
51. Baran, D. T. & Kelly, A. M. Lysophosphatidylinositol: a potential mediator of 1,25-dihydroxyvitamin D-induced increments in hepatocyte cytosolic calcium. *Endocrinology* **122**, 930–934 (1988).
52. Quan, C. et al. Impaired SERCA2a phosphorylation causes diabetic cardiomyopathy through impinging on cardiac contractility and precursor protein processing. *Life Metab.* **1**, 54–66 (2022).
53. Zhang, Y. et al. Cardiomyocyte PKA ablation enhances basal contractility while eliminates cardiac beta-adrenergic response without adverse effects on the heart. *Circ. Res.* **124**, 1760–1777 (2019).
54. Hirano, Y., Moscucci, A. & January, C. T. Direct measurement of L-type Ca2+ window current in heart cells. *Circ. Res.* **70**, 445–455 (1992).
55. Ames, B. N. Assay of inorganic phosphate, total phosphate and phosphatase. *Methods Enzymol.* **8**, 115–118 (1966).
56. Shui, G. et al. Derivatization-independent cholesterol analysis in crude lipid extracts by liquid chromatography/mass spectrometry: applications to a rabbit model for atherosclerosis. *J. Chromatogr. A* **1218**, 4357–4365 (2011).
57. Quan, C. et al. SPEG controls calcium reuptake into the sarcoplasmic reticulum through regulating SERCA2a by its second kinase-domain. *Circ. Res.* **124**, 712–726 (2019).


## Acknowledgements

We thank Prof. Carol MacKintosh (University of Dundee, UK) for proofreading the manuscript and members of the resource unit at Nanjing University for technical assistance. Thanks to the Ministry of Science and Technology of China (Grant Nos. 2021YFF0702100 and 2018YFA0801100 to S.C. and H.-Y.W.), the National Natural Science Foundation of China (Grant Nos. 32025019 to S.C.), the Science and Technology Foundation of Jiangsu Province of China (Grant No. BK20243041 (Key Research Program) to S.C. and H.-Y.W.), and the Fundamental Research Funds for the Central Universities (021414380533 to S.C., 021414380505 to Q.L.C., and 021414380508 to C.Q.), for financial support.

## Author contributions

S.S., C.Q., Q.L.C., R.Z.W., Q.D., S.S.Z., M.L., X.Y.Y., P.R., J.C., Y.Y.B., W.Z., W.K.F., M.J.L., B.X.X., K.F.O.Y., Y.S.S., F.L., X.Q.Z., R.P.X., and X.W.C. performed experiments, analyzed data and reviewed the manuscript. H.-Y.W. and S.C. designed experiments, analyzed data, and wrote the manuscript. S.C. is the guarantor of this study.

## Competing interests

The authors declare no competing interests.

## Additional information

**Supplementary information** The online version contains supplementary material available at https://doi.org/10.1038/s41467-024-54031-5.

**Correspondence** and requests for materials should be addressed to Hong-Yu Wang or Shuai Chen.

**Peer review information** *Nature Communications* thanks the anonymous reviewers for their contribution to the peer review of this work. A peer review file is available.



[1]State Key Laboratory of Pharmaceutical Biotechnology, Department of Cardiology, Nanjing Drum Tower Hospital, The Affiliated Hospital of Nanjing University Medical School, Model Animal Research Center, School of Medicine, Nanjing University, Nanjing, China. [2]MOE Key Laboratory of Model Animal for Disease Study, Department of Endocrinology, Nanjing Drum Tower Hospital, The Affiliated Hospital of Nanjing University Medical School, Model Animal Research Center, School of Medicine, Nanjing University, Nanjing, China. [3]Department of Neurology, Nanjing Drum Tower Hospital, Affiliated Hospital of Medical School, Nanjing University, Nanjing, China. [4]Department of Biopharmaceuticals & Tianjin Key Laboratory on Technologies Enabling Development of Clinical Therapeutics and Diagnostics, School of Pharmacy, Tianjin Medical University, Tianjin, China. [5]Institute of Molecular Medicine, College of Future Technology, Peking University, Beijing, China. [6]Beijing Key Laboratory of Cardiometabolic Molecular Medicine, Peking University, Beijing, China. [7]Department of Cardiovascular Surgery, Peking University Shenzhen Hospital, Shenzhen, China. [8]Beijing Laboratory for Cardiovascular Precision Medicine, MOE Key Laboratory of Biomedical Engineering for Cardiovascular Disease Research, Beijing Anzhen Hospital, Capital Medical University, Beijing, China. [9]Nanjing Biomedical Research Institute, Nanjing University, Nanjing, China. [10]Nanjing Key Laboratory for Cardiovascular Information and Health Engineering Medicine, Nanjing, China. [11]These authors contributed equally: Shu Su, Chao Quan, Qiaoli Chen. [12]These authors jointly supervised this work: Hong-Yu Wang, Shuai Chen. ✉e-mail: wanghy@nicemice.cn; chenshuai@nju.edu.cn